Journal of Geophysical Research: Oceans

RESEARCH ARTICLE
10.1002/2017JC013390

Gulf Stream Transport and Mixing Processes via Coherent Structure Dynamics

Yi Liu[1,2], Chris Wilson[3], Melissa A. Green[1], and Chris W. Hughes[3,4]

[1]Department of Mechanical and Aerospace Engineering, Syracuse University, Syracuse, NY, USA, [2]Now at Department of Aerospace and Mechanical Engineering, University of Notre Dame, Notre Dame, IN, USA, [3]National Oceanography Centre, Liverpool, UK, [4]School of Environmental Sciences, University of Liverpool, Liverpool, UK

Key Points:
- Lagrangian and Eulerian diagnosis of altimetry observations are used to explore and compare new and existing jet and transport paradigms
- Lagrangian coherent structures (LCS) show that the Bower kinematic model holds only locally and intermittently in the unstable jet region
- The jet pinch-off process is linked to the wave-maker jet region. Lobe dynamics and pinch-off may each account for gross transport ~10 Sv

Supporting Information:
- Support Information S1
- Movie S1

Correspondence to:
Y. Liu,
yliu27@nd.edu

Citation:
Liu, Y., Wilson, C., Green, M. A., & Hughes, C. W. (2018). Gulf Stream transport and mixing processes via coherent structure dynamics. *Journal of Geophysical Research: Oceans*, *123*. https://doi.org/10.1002/2017JC013390

Received 13 SEP 2017
Accepted 25 MAR 2018
Accepted article online 6 APR 2018

Abstract The Gulf Stream has been characterized as either a barrier or blender to fluid transfer, a duality relevant to gyre-scale climate adjustment. However, previous characterization depended on relatively sparse, Lagrangian in situ observations. The finite-time Lyapunov exponent (FTLE) is calculated from satellite altimetry to identify Lagrangian coherent structures (LCS) in the Gulf Stream region. These LCS provide dense sampling of flow and capture distinct regions associated with mixing. Independent observations of ocean color contain similar flow-dependent structures, providing verification of the method and highlighting transport and mixing processes that influence sea surface temperature and chlorophyll, among other water properties. Diagnosed LCS support the existing Bower kinematic model of the Gulf Stream, but also highlight novel behavior of comparable importance. These include vortex pinch-off and formation of spiral eddies, clearly identified by LCS and which may be explained by considering changes to flow topology and the dynamics of shear-flow instability at both small and large Rossby number. Such processes, seen though LCS, may further enable validation of climate models. The spatial distribution of these intermittent processes is characterized in terms of the criticality of jet dynamics with respect to Rossby wave propagation, and whether the jet is in an unstable or wave-maker regime. The generation and connectivity of hyperbolic trajectories in the flow appears to play an important role in governing large-scale transport and mixing across the Gulf Stream.

Plain Language Summary Earth is heated by the sun more strongly near the equator than near the poles. The atmosphere and ocean dynamics redistribute this heating imbalance via fluid transfer to achieve a climate that is more moderate and less extreme. At midlatitudes, the ocean transports more heat poleward than the atmosphere, and the physical processes in the Gulf Stream affect the rate of heat transport for the North Atlantic. Changes in heat transport set ocean surface temperature patterns, which affect atmospheric weather and also govern climate variability. These crucial transport processes involve the interaction of the Gulf Stream with ocean eddies, typically tens of kilometers in diameter, the ocean's equivalent of atmospheric weather systems. This study uses the latest satellite observations and a new method for identifying structures in fluid flow to reexamine a picture of the transport processes, first developed 30 years ago. In order to accurately predict future global climate, computer simulations need to represent these key transport processes at ocean eddy scales. We show that the traditional view is still relevant for part of the Gulf Stream, but that fascinating new behavior is also seen from space, showing the generation and evolution of flow structures central to fluid transport.

1. Introduction

North Atlantic climate and its dynamical adjustment depend significantly on material and other scalar transport across the Gulf Stream, connecting key sources and sinks of dissolved carbon, heat content, mass, and potential vorticity. At Gulf Stream latitudes between 20°N and 38°N, mesoscale eddies account for up to two-thirds of the variability of the large-scale Meridional Overturning Circulation (MOC), dropping to one-third at other latitudes (Thomas & Zhai, 2013). The northward heat transport of 1.25 PW observed at 26°N is dominated by, and closely corresponds with, the overturning component of the MOC, with the gyre component only accounting for 10% of the total (McCarthy et al., 2015). Rypina et al. (2011) use a very approximate

estimate, 10% of alongstream transport, to suggest that there is 6.5 Sv near-surface transport across the Gulf Stream from the subtropical to subpolar gyre, due to wind-driven and eddy-driven flow.

The traditional "Conveyor Belt" model of the MOC, which is fundamentally an oversimplified view, has been expanded using Lagrangian float observations and ocean modeling (Bower et al., 2009) to uncover the complex pathways of transport and mixing that play an important role in climate adjustment. The dynamics of the Gulf Stream are an important component of the MOC, both in the equatorward transport of the lower limb of the MOC through interior pathways of Labrador Sea Water (Bower et al., 2009), and the poleward transport of the upper limb from subtropical to subpolar gyre (Rypina et al., 2011). Both these examples point to the importance of the time-varying flow and to so-called "hot spots," where transport and mixing is largest. It is becoming clearer that understanding the nature of Gulf Stream transport and mixing, and representing these processes correctly in climate models, is crucial in order to simulate changes to the MOC and climate. (In this paper we resolve effects due to stirring but use "mixing" to describe them, with the understanding that in realistic flows with small-scale dissipation of properties such as momentum or tracers, the stirring generates small flow scales which lead ultimately to property mixing.)

Kinematic models have been developed (Bower, 1991; Samelson, 1992), based on sparse, Lagrangian float observations (Bower & Rossby, 1989), and illustrate that different regions of the Gulf Stream may either enhance or inhibit transport and mixing (Bower et al., 1985). It is timely to update the understanding of the surface Gulf Stream using the broad coverage of satellite observations. The recently derived Segment-Sol multimissions d'ALTimétrie, Orbitographie et localisation précise/Data Unification and Altimeter Combination System (SSALTO/DUACS) absolute dynamic topography and absolute geostrophic velocity products (www.aviso.altimetry.fr) are constrained by multiple satellite altimeter and gravity missions. The gridded products have an effective spatial resolution equivalent to $\sim$180 km wavelength (p12 of Pujol and SL-TAC Team, 2017) or length scale (wavelength/2π) $\approx$ 30 km, and therefore resolve the upper end of the ocean mesoscale in the Gulf Stream region (i.e., able to resolve a first baroclinic Rossby deformation radius of $\sim$30 km for which the corresponding Rossby waves would have wavelength $\sim$180 km; Chelton et al., 1998).

As highlighted by d'Ovidio et al. (2009), there are many examples illustrating how diagnostics derived from Lagrangian analysis of the satellite altimetry geostrophic velocity fields may capture information at the altimetry gridscale. In fact, ridges of scalar Lagrangian fields often have widths that are sharp and much narrower than the data gridscale, but the size of the dynamic structures they can distinguish is still limited to the spatial scale of the data. Analogous to a tracer field, Lagrangian diagnostics contain time-integrated effects of the spatial flow structures, for example, the history of straining and folding of material (see Marshall et al., 2006, for a tracer-altimetry example), like manual kneading of bread dough where the external forcing is larger-scale than the material structures that are developed. Moreover, such Lagrangian diagnostics are relatively insensitive to the comparably coarse spatial and temporal resolution of satellite altimetry or the method used to interpolate velocity to a finer grid (Harrison & Glatzmaier, 2012). More formally, a Lagrangian method that uses the finite-time Lyapunov exponent (FTLE) was shown to be relatively insensitive to errors in the velocity field that are small in a special time-weighted norm (Haller, 2002). The weight function in this norm turns out to decay exponentially in time, allowing for temporally localized spikes in the error in both the velocity and its gradient.

Lagrangian methods, such as FTLE and finite-size Lyapunov exponent (FSLE), have further advantages over Eulerian methods like the commonly used Okubo-Weiss (OW) criterion (e.g., Isern-Fontanet et al., 2006; Chelton et al., 2007), in that they are also objective (frame-invariant) and that the identification of structures does not depend on a choice of threshold. Additional techniques have been introduced that implement a variety of theories to ensure the accuracy of coherent patterns observed in Lagrangian analysis, including the variational theory method proposed by Haller (2011) and the three-dimensional braid structure construction developed by Allshouse and Thiffeault (2012) in an attempt to rectify errors in the flow map caused by the low number of trajectories common to oceanic flows sampled by floats and drifters.

Further investigation determined that in two-dimensional turbulent flows these Lagrangian coherent structures can travel through the flow without being destroyed (Haller & Beron-Vera, 2012, 2013). In large-scale oceanic flows, coherent structures such as vortices can persist over long periods of time and can collect surface material such as surfactant, garbage or oil into a persistently concentrated region. This type of analysis has since been extended to three-dimensional unsteady flows in an investigation of hyperbolic and elliptic

transport barriers (Blazevski & Haller, 2014). Most recently, Haller et al. (2016) have developed the Lagrangian Averaged Vorticity Deviation (LAVD) and the Instantaneous Vorticity Deviation (IVD) as a means of identifying objective coherent vortices from both Lagrangian and Eulerian calculations.

The aims of this study are:

1. To develop a more complete understanding of ocean transport and mixing processes, particularly in relation to the Gulf Stream, but with the hope of also connecting with similar studies of other regions containing ocean jets and eddies, for example, in the Kuroshio and the Antarctic Circumpolar Current, where the ocean mesoscale is also known to interact strongly with large-scale ocean dynamics.
2. To test both Lagrangian and Eulerian paradigms of the Gulf Stream, and to see how they relate to each other and are constrained by observations.

This work is an initial, largely qualitative study of the phenomena, with the aim of refining the questions to be addressed by more formal and quantitative techniques in the future.

Across the different methods of Lagrangian analysis, the goal is the detection and tracking of coherent patterns, motions, and structures in time and space. Generally, these features are referred to as Lagrangian coherent structures (LCS). In this paper, we will use the ridges of the finite-time Lyapunov exponent (FTLE) to characterize the flow structures in and around the Gulf Stream. There have been several other recent ocean applications of FTLE (Coulliette et al., 2007; Harrison & Glatzmaier, 2012; Lekien et al., 2005; Olascoaga et al., 2006, 2008) and FSLE (d'Ovidio et al., 2004, 2009) including comparison of identified flow structures with Lagrangian surface drifter paths (Beron-Vera et al., 2008; Shadden et al., 2009). Du Toit (2010) also applied FTLE to study the transport mechanisms induced by mesoscale eddies in the ocean. While the Gulf Stream has been included in global studies (Beron-Vera et al., 2008; Du Toit, 2010; Waugh & Abraham, 2008), it has not yet been the focus of any studies, except by Rypina et al. (2011) who studied transport over a much longer time ($\mathcal{O}$(years)) than that presented here ($\mathcal{O}$(days)). Our focus is on the surface, geostrophic dynamics of the Gulf Stream and its flow characteristics governing material transfer, as captured by the latest SSALTO/DUACS absolute geostrophic velocity time series. We explore both the spatial and temporal characteristics of the Gulf Stream and identify LCS in the context of an existing kinematic jet model and a classic shear-flow instability.

2. Method

There have been several Lagrangian metrics developed to study flow structure and coherence, and in the work presented here, the FTLE method is used. FTLE is a scalar field that measures the rate of separation of neighboring fluid particle trajectories starting from that point. At time t, the flow map $\phi(\boldsymbol{x}_0, t_0+T, t_0)$ denotes the position of a fluid particle trajectory initialized at position $\boldsymbol{x}_0$ and time t_0. Then FTLE at position $\boldsymbol{x}_0$ and time t_0, found using integration time T, is defined by,

$$\mathrm{FTLE}(\boldsymbol{x}_0, t_0, T) = \frac{1}{2T} \log \sigma(\boldsymbol{x}_0, t_0, T), \tag{1}$$

where σ is the maximum eigenvalue of the right Cauchy-Green deformation tensor, defined as,

$$\sigma(\boldsymbol{x}_0, t_0, T) = \lambda_{\max}\left(\left[\frac{\partial \phi(\boldsymbol{x}_0, t_0+T, t_0)}{\partial \boldsymbol{x}_0}\right]^* \left[\frac{\partial \phi(\boldsymbol{x}_0, t_0+T, t_0)}{\partial \boldsymbol{x}_0}\right]\right). \tag{2}$$

Here T is the time difference between the initialization time t_0 and measuring time t, and $[]^*$ indicates the matrix transpose.

The eigenvalues of the Cauchy-Green tensor theoretically represent the stretching and compression of the fluid area (in 2-D) or volume (in 3-D). In this work, where the flow representation is 2-D, the FTLE quantifies the stretching along the relevant direction. In 3-D, there are potentially two axes of stretching, and by taking the maximum eigenvalue, the FTLE quantifies the maximum stretching, with the direction identified by the eigenvector associated with that eigenvalue. Regions of locally maximal stretching can be revealed by the maximizing ridges of FTLE fields, and these ridges are referred to as LCS in the current work. We can calculate both positive-time ($T>0$) and negative-time ($T<0$) FTLE fields (pFTLE and nFTLE) at a time t_0, by integrating trajectories in positive-time and negative-time, respectively. This is consistent with the

"standard" method, as referred to by Lipinski and Mohseni (2010). While flow maps integrated in positive and negative-time from t_0 technically cover different spans of time, the integration time is short relative to the time scales of the structure evolution, and therefore the two FTLE fields calculated in this way are expected to capture the same structures at their location at t_0. For reference, an integration time of 6 days is predominantly used in this study, while Du Toit (2010) used 3 weeks, and Rypina et al. (2011) used 2 years.

From these, we extract positive-time and negative-time LCS (pLCS and nLCS) by thresholding the respective FTLE fields to only those ridges with values over 50% of the global maximum over the whole time series. Typically 50–80% of the maximum FTLE value has been shown to be an adequate choice (Lipinski, 2012). We demonstrate in section 3 that the dominant flow structures identified by our method are not sensitive to threshold choice or integration time. The maximizing ridges of pFTLE field represent large local stretching among particle trajectories starting at the same time, so pLCS may indicate repelling lines of the flow. The nFTLE field reveals stretching among particle trajectories integrated in negative-time also, indicating that the trajectories have been converging. Large magnitudes of nFTLE field represent large local attraction, and its ridges may indicate attracting lines. The superposition of both types of LCS represent kinematically distinct regions of fluid attraction and repulsion, and are useful for studying transport and mixing properties of oceanic flows.

The elliptic, hyperbolic, and parabolic curves that one acquires from the variational theory approach of LCS are admittedly more mathematically rigorous and well-defined than a generic approach involving FTLE (Farazmand & Haller, 2012). The variational methods were implemented using the available toolbox (Onu et al., 2015), and it was found that the variational LCS are extremely sensitive to the parameters used in the calculation, including the size of the domain, the integration time, and the filtering parameter values ℓ_f and $\ell_{\min}$. When implementing the variational theory LCS, it was necessary first to decrease the domain size greatly for memory management within Matlab, and even then it was not possible to consistently identify lobes of the Gulf Stream meanders that are clearly associated with material transport in the images of SST and chlorophyll below in Figure 2. It was noted, however, that when calculating the FTLE field with the same toolbox, the FTLE ridges were relatively robust to the same set of parameters. For this application, we therefore conclude that our FTLE approach is appropriate.

3. Velocity and Dynamic Topography Data

For this study, SSALTO/DUACS (www.aviso.altimetry.fr) all-satellite, merged, DUACS2014 absolute geostrophic velocity product (MADT-UV) and absolute dynamic topography (MADT-H) are used. The velocity and dynamic topography are provided on a 0.25° latitude-longitude grid, at daily interval, derived through optimal interpolation of up to four satellites at any instant, having been calculated from the absolute dynamic topography (sea level relative to the geoid) using geostrophic balance. Ekman layers and other ageostrophic effects are ignored for simplicity. Our domain includes the Gulf Stream and North Atlantic Current, 90–30°W and 25–55°N, and covers 1 January 1993 to 24 October 2014.

The velocity field derived from altimetry data is interpolated onto a finer space-time grid using trilinear interpolation for FTLE calculation. The finer grid has 5 times the spatial resolution in both directions (i.e., grid size of 0.05° latitude-longitude) and 3 times the temporal resolution (i.e., time step of one-third a day) of the original grid. Then, a classical fourth-order Runge-Kutta method is performed on the finer grid to obtain the flow map $\phi(\boldsymbol{x}_0, t_0+T, t_0)$, with integration time $T=6$ days (for pFTLE) and $T=-6$ days (for nFTLE). Both the pFTLE and nFTLE fields are calculated using (1). The increased spatial resolution of the FTLE provides a sharper visualization of the LCS ridges, but does not on its own increase the resolution of the observed structures.

The LCS example from Figure 1 is derived from the SSALTO/DUACS absolute geostrophic velocity on 18 April 2005 and shows pFTLE and nFTLE calculated using integration time of both $T=6$ days and $T=12$ days. Although the $T=12$ days example captures more fine structure and rollup, we consider $T=6$ days to be appropriate for Gulf Stream flow where the typical e-folding growth period for mesoscale eddies is 15–25 days in the upper ocean (Williams et al., 2007). Note also that the maximizing FTLE ridges in Figure 1, based on $T=6$ days capture the dominant structures in the full FTLE fields for both $T=6$ days and $T=12$

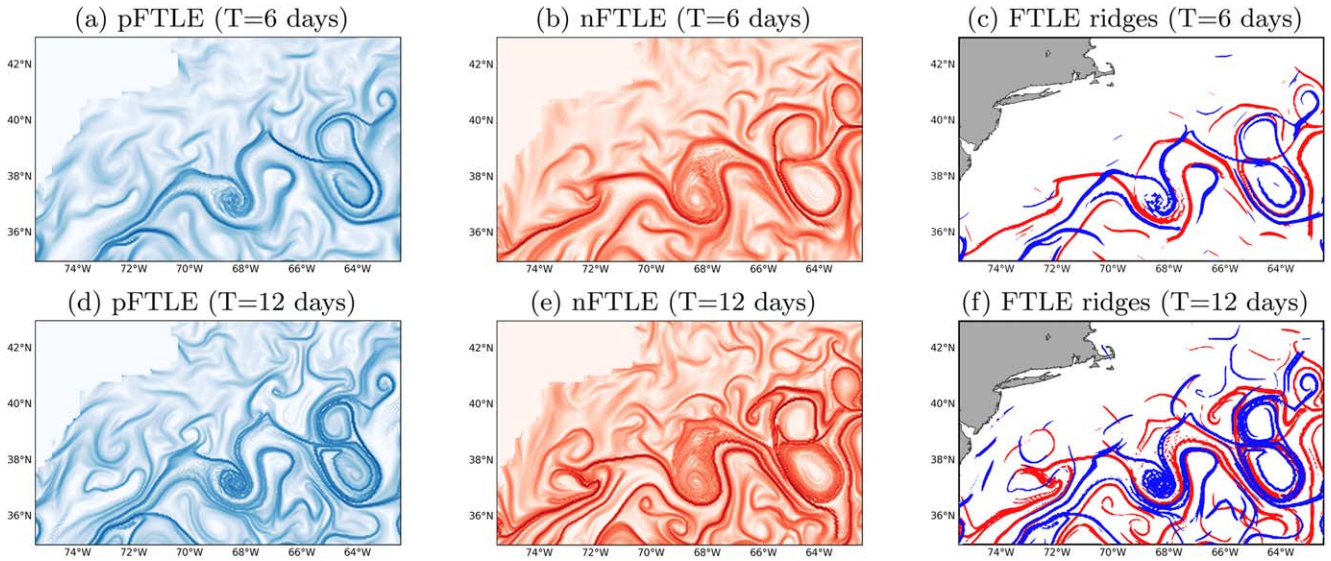

Figure 1. Composition of the finite-time Lyapunov exponent field for two different integration times, each calculated from satellite-derived surface geostrophic velocity in the Gulf Stream region, centered on 18 April 2005. For an integration time of 6 days, (a) pFTLE and (b) nFTLE highlight regions with strong flow trajectory divergence and convergence, respectively. (c) An overlay of their maximizing ridges, highlighting pLCS (blue) and nLCS (red). Similar flow diagnostics are shown for an integration time of 12 days: (d) pFTLE, (e) nFTLE, and (f) their maximizing ridges, as pLCS (blue) and nLCS (red). Note that the dominant features in LCS in Figure 1c are also present in Figure 1f. See text for more details.

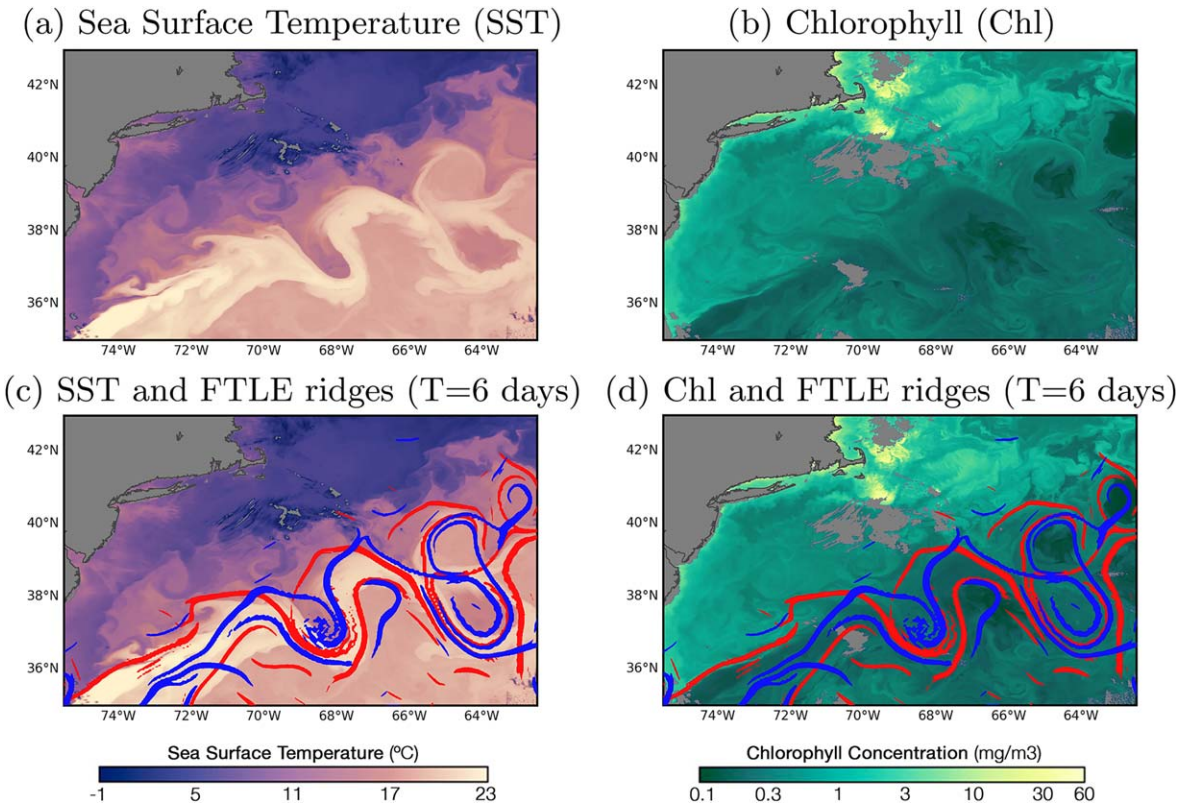

Figure 2. Observations of (a) sea surface temperature (SST) and (b) chlorophyll concentration (Chl) at 1 km lateral resolution in the Gulf Stream on 18 April 2005, made from data collected by the Moderate Resolution Imaging Spectroradiometer (MODIS) on NASA's Aqua satellite. These independent MODIS observations contain structures that align with pFTLE (blue) and nFTLE (red) ridges, as overlaid on (c) SST and (d) Chl, respectively. The chlorophyll image had a filter applied to shift its color for presentation purposes.

days. We further examined the FTLE ridges for a range of T from 2.4 to 9 days in 0.6 day increments and found that $T = 6$ days was sufficient to extract the main features. In the third column, the two scalar fields are thresholded at 50% of the global maximum as described previously and superimposed. Again, while some additional ridges or extensions of existing ridges are obvious, no additional dynamics can be educed from results using the longer integration time.

Compelling evidence of the ability of LCS calculated in this way (SSALTO/DUACS-derived) to capture Gulf Stream dynamics is provided by independent (MODIS-derived) satellite observations of sea surface temperature (SST) and chlorophyll concentration (Chl) (Figure 2). SST acts as a quasi-conserved flow tracer. Observed SST (Figure 2a) shows the cold water located poleward of the Gulf Stream (which is highlighted as a tongue of water warmer than 20°C). Equatorward, water is colder than in the Gulf Stream, but warmer than the rest of the domain. Although Chl depends also on biogeochemical processes, similar structures are seen, due to the shared physics governing the flow (Figure 2b).

Both pFTLE and nFTLE ridges align closely with a large proportion of the SST (Figure 2c) and Chl (Figure 2d) structure. It is reassuring that the MODIS data, with nominal 1 km resolution, confirms LCS derived from SSALTO/DUACS data, even at scales smaller than its effective 30 km resolution.

4. Eulerian Context

In order to interpret the Lagrangian diagnostics, it is useful to have in mind a picture of the spatially varying Eulerian dynamical regimes of the Gulf Stream. Figure 3 shows the mean dynamic topography over the period considered (color), with contours of bathymetry superimposed. A number of different regions are apparent. Initially, the Gulf Stream flows in water shallower than 1,000 m, along the Florida coast, until it crosses the continental slope in the vicinity of Cape Hatteras (about 35°N). Following this, it turns steadily more to the east, initially remaining almost as narrow as before, and developing a pair of recirculating gyres to the north and south. These gyres reach peak strength at about 70–71°W, at which point the main jet starts to spread. Between about 65°W and 62°W, the jet encounters the New England Seamounts (NESM),

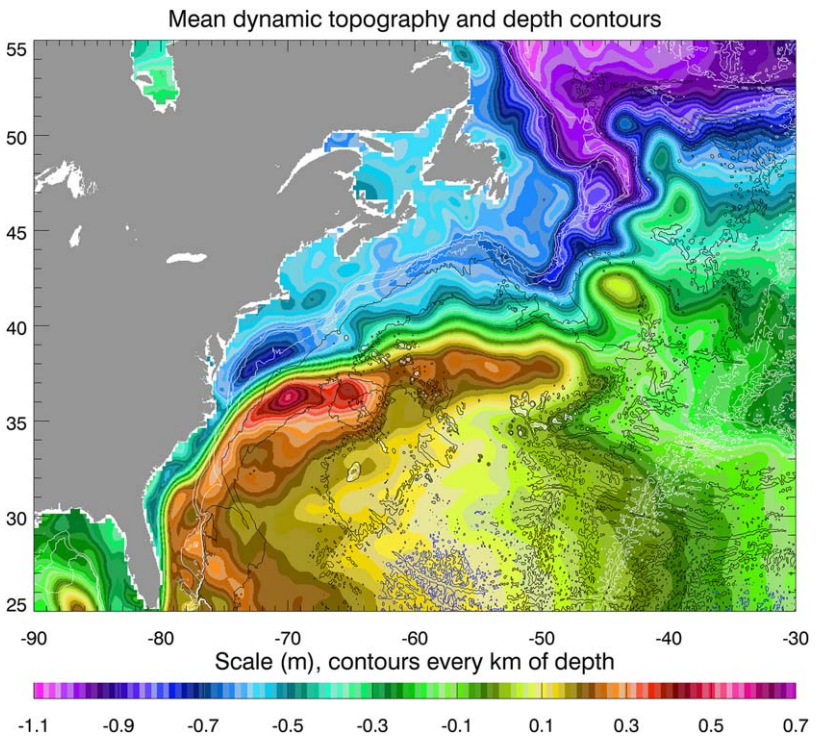

Figure 3. The mean dynamic topography in the Gulf Stream region (color), with bathymetry contoured on top. Bathymetry contours are (white) 1, 2, 3 km; (black) 4, 5 km; (blue) 6 km.

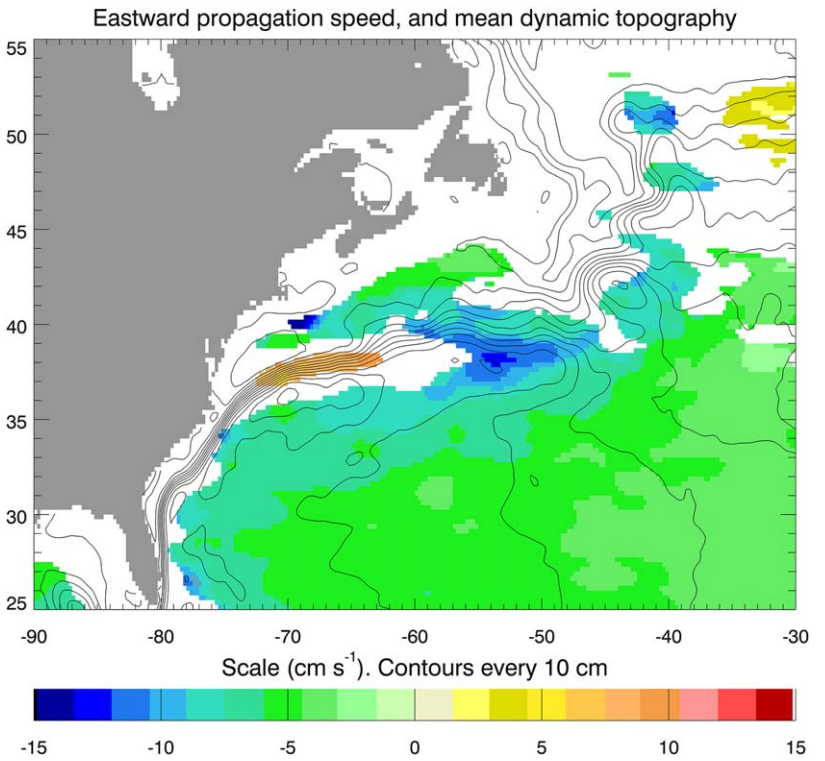

Figure 4. The dominant zonal propagation speed of mesoscale features in the dynamic topography (color), with mean dynamic topography contoured on top. White regions show where no clear propagation speed is obtained. Positive speeds are to the east.

seen here as small patches of white contours where the depth is less than 3,000 m. At this point the jet broadens suddenly, and starts to flow almost zonally, but with standing meanders, and some apparent steering by the deep topography in this region.

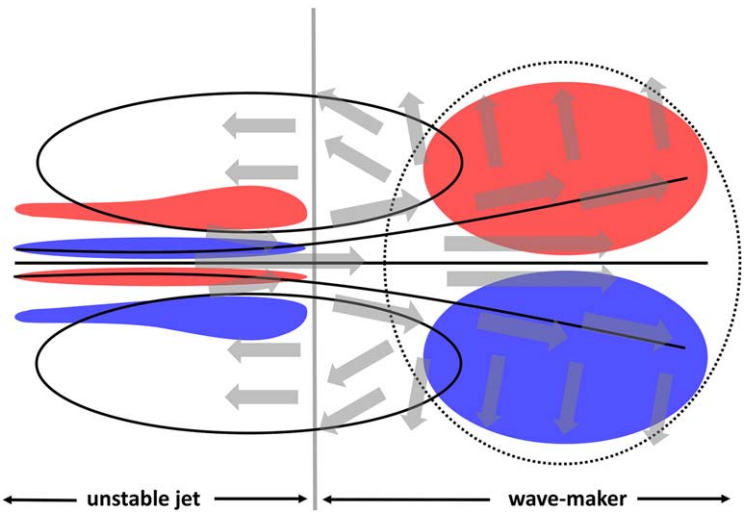

Figure 5. Schematic showing aspects of the eddy-mean flow interaction in the core of an idealized Gulf Stream-like jet flow, adapted from Figures 1 and 5b of Waterman and Hoskins (2013). Black solid lines are streamlines, with the flow from east to west in the center, and with recirculations to the north and south of the jet. The black dotted line encompasses the main wave-maker region, and the vertical gray line marks the longitude of greatest recirculation, coincident with the end of the unstable jet region. Red represents regions where the eddy vorticity flux divergence acts as a source of vorticity to the mean flow, and blue where it acts as a sink. Gray arrows show the approximate direction of eddy (or wave) energy flux.

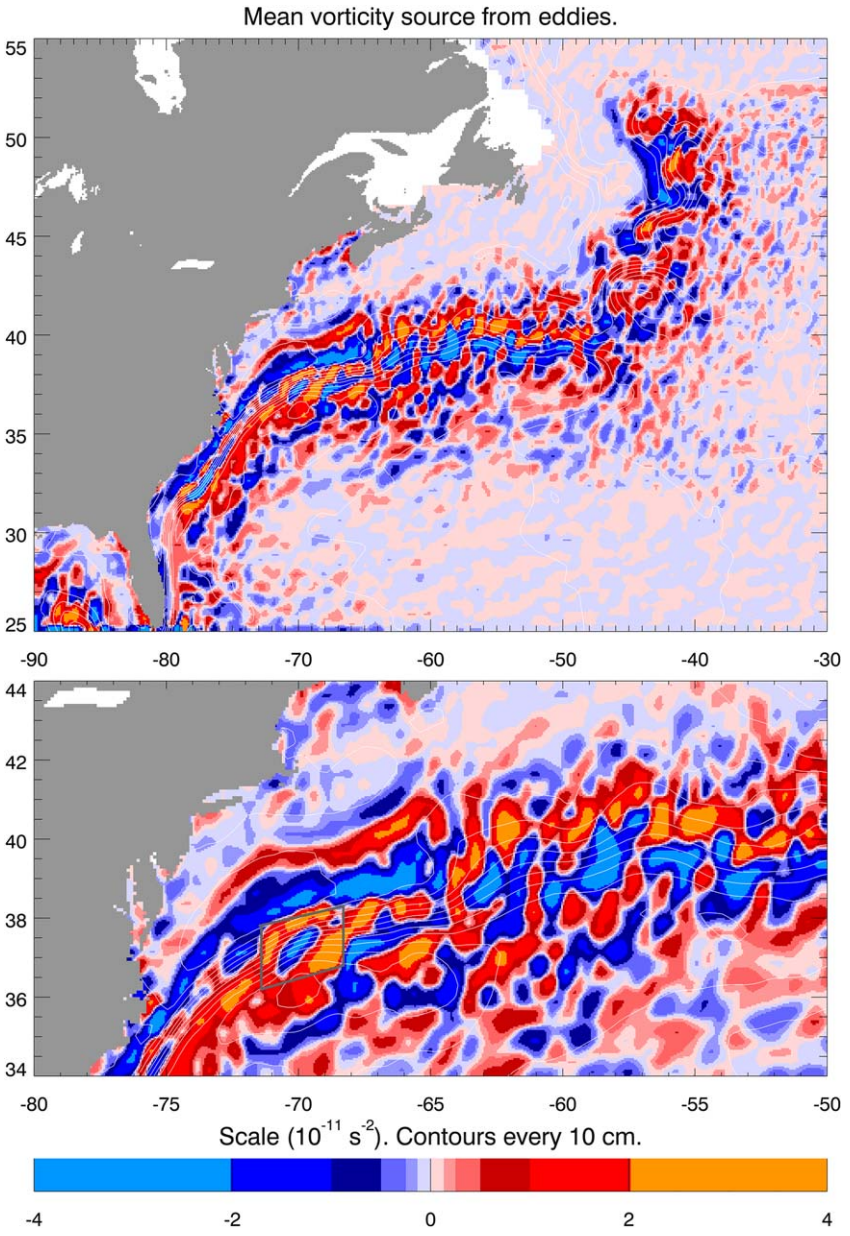

Figure 6. The mean source of vorticity in the mean flow, due to eddies (color), with the mean dynamic topography contoured on top in white. The bottom plot is an expanded version of the top plot. The gray box represents a broad transition zone from unstable jet to wave-maker region, equivalent to the sharper transition represented by the gray line in Figure 5.

In Figure 4, we show the dominant zonal propagation speed of mesoscale sea level anomalies, calculated using a Radon transform as described in Smith and Marshall (2009). This shows how the stretch between Cape Hatteras and the NESM is unusual in that disturbances propagate to the east here, showing that the flow speed is supercritical with respect to Rossby wave propagation. Elsewhere, including in the Gulf Stream to the east of the seamounts, the natural westward propagation of Rossby wave dynamics is dominant and the flow speed is subcritical. White regions show where no consistent zonal propagation can be identified.

The idealized studies of Waterman and Jayne (2011) and Waterman and Hoskins (2013) provide a useful context for interpretation of the supercritical part of the Gulf Stream. Figure 5, an amalgamation of parts of Figures 1 and 5b from Waterman and Hoskins (2013), summarizes the complex interactions involved. The jet is barotropically unstable upstream of the maximum recirculation (gray line). In this region, eddies act as

a source of vorticity (red) in the southern part of the jet, and a sink (blue) in the northern part, with complementary effects in the recirculations. Downstream of the maximum recirculation, where the jet broadens, is the "wave-maker" region, from which eddies radiate energy. Here there is a broader vorticity sink to the south, and a source to the north, as eddies flux vorticity across the jet from south to north.

The gray arrows in Figure 5 summarize the direction of eddy energy flux, showing that this is to the east throughout the core of the jet (with a component into the jet in the instability region), radiating out to north and south in the wave-maker region, and turning back to the west to either side of the jet. This picture is compatible with Figure 4 for the supercritical region between Cape Hatteras and the NESM.

Figure 6 shows the convergence of eddy vorticity flux as diagnosed from the satellite velocities, MADT-UV. To be precise, what is shown is $-\nabla\cdot(\overline{\mathbf{u}'\zeta'})$, where $\mathbf{u}'$ is the high-pass filtered velocity, passing periods shorter than 6 months, and ζ' is the high-pass filtered relative vorticity derived from the same velocities. The overline represents a time average. As in the schematic Figure 5, red represents a source of vorticity to the mean flow from the eddies ($-\nabla\cdot(\overline{\mathbf{u}'\zeta'})>0$), and blue a sink.

The only region where the jet contains blue in its northern half and red in its southern half as expected in the unstable jet region, is shortly after turning away from Cape Hatteras, in the region 73°W to 72°W. From 68°W onward, excluding the NESM, the pattern has generally reversed, as expected in the wave-maker region. However, the transition between these two regimes (shown by a gray box in Figure 6) is characterized by a series of diagonal stripes across the current rather than the simple switch shown in Figure 5, perhaps a result of the nonzonal nature of the jet in this region. The jet starts to broaden and the recirculations to weaken at about 70°W, in the middle of the transition region. Downstream of the NESM (east of about 64°W), the broader jet continues to be generally red to the north and blue to the south, as in the wave-maker region, but the westward propagation of mesoscale features shows that this is beyond the region considered by Waterman and Hoskins (2013).

In summary, we interpret the Gulf Stream system as having four regimes. There is an initial, strongly topographically steered regime before reaching Cape Hatteras, an unstable jet regime followed by a wave-maker regime in the supercritical flow region between Cape Hatteras and the NESM, and a subcritical wave-maker regime downstream of the NESM. It will be interesting to consider how the different regimes are reflected in Lagrangian diagnostics.

5. Lagrangian Results

Both pFTLE and nFTLE are calculated in the Gulf Stream region over a 22 year period. The most obvious coherent structures that the FTLE ridges identify include: the main jet structure of the Gulf Stream; strong spiral vortices that grow, interact, and decay near the Gulf Stream; and weaker vortex structures, identified by LCS intersections (LCS saddles) that propagate westward at approximately the long baroclinic Rossby wave phase speed within the ocean interior east of the Gulf Stream and North Atlantic Current (Figure 7 and the full 22 year movie, supporting information Movie S1). Both the boundaries of the jet core and the cyclonic and anticyclonic vortices generated on flanks of the jet stream are outlined by FTLE ridges. It is known that both jet meandering and vortex-jet interaction are important mechanisms of fluid exchange between the Gulf Stream and its surroundings (Song et al., 1995). Such exchanges are highlighted by the LCS shown here.

5.1. Kinematics of Entrainment and Detrainment in a Jet With Propagating Meanders

One important mechanism of fluid exchange between the Gulf Stream and its surroundings is associated with Gulf Stream meanders (Bower & Rossby, 1989). To observe this, we focus on the region where the jet is strongest and has just separated from the coast near Cape Hatteras, highlighted in the inset in Figure 7a. Just east of Cape Hatteras, 75–68°W, the Gulf Stream has meanders (traveling wave structures) that propagate eastward. Further downstream, at around 68–60°W, there are standing meanders that have large meridional excursions (see also Cornillon, 1986) and that are frequently pinched-off to form separate eddies (Fuglister & Worthington, 1951). In the upstream region where lateral shear is strongest, barotropic instability dominates, but further downstream, as in the ocean interior, baroclinic instability takes over. Here the first aim is to test an established kinematic model of the Gulf Stream and its eastward-propagating

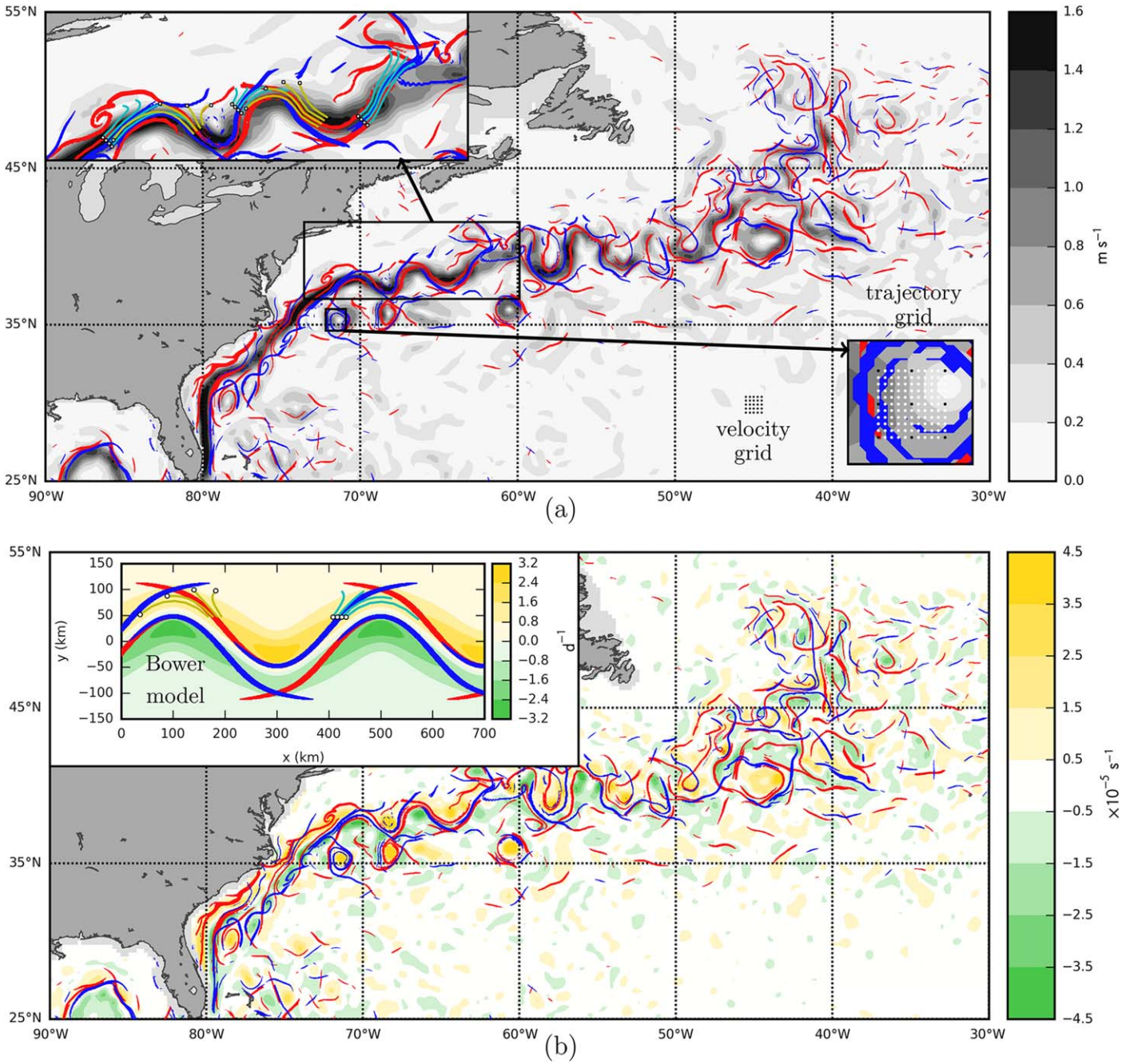

Figure 7. (a) Velocity magnitude and (b) relative vorticity in the Gulf Stream region on 7 March 2003, superimposed with pFTLE (blue) and nFTLE (red) ridges. Top left inset in Figure 7a shows 3 day positive-time (cyan) and negative-time (yellow) trajectories with initialization points for forward time progression indicated by a white circle. Black and white dots in the bottom right inset of (a) show spatial resolution of the velocity and trajectory grids, respectively. Top left inset in Figure 7b is relative vorticity of the Bower model of jet entrainment/detrainment, superimposed with FTLE ridges and sample particle trajectories, as in Figure 7a. Details of the Bower model are described in the text.

meanders against observed LCS and, in the following two subsections, to put forward mechanisms for the dynamical and topological generation of the remaining types of LCS that are observed.

Figure 7a shows ridges of pFTLE (blue) and nFTLE (red) of the ocean surface in the Gulf Stream region on one representative day (7 March 2003), together with the velocity magnitude in that region (contours increasing from white to black). FTLE ridges are located on both flanks of the jet. More specifically, we can see alternating pFTLE and nFTLE ridges along both the poleward and equatorward flanks, indicating the

regions of past entrainment and future detrainment. Local fluid attraction (entrainment) occurs along the leading edges of the meander crests (red attracting nFTLE ridges) while the dividing line between fluid that has been entrained into the main jet and that which is leaving the main jet (detrainment) is located along the back side (or trailing edge) of the meander crests (blue repelling pFTLE ridges).

Trajectories of several advected tracer particles are also included in the inset of Figure 7a to show the pathways of fluid exchanges. Cyan lines in the figure are trajectories initialized on 7 March 2003 and integrated in positive-time, while yellow lines are trajectories that were identified in a negative-time integration over the previous three days to indicate the ongoing fluid attraction along the nFTLE ridge. The white dots attached to the yellow lines indicate where trajectories started three days prior to 7 March 2003. As indicated by the yellow and cyan lines, the relative motion of trajectories near the boundary of the jet are consistent with cyclonic relative vorticity in the troughs of U-shaped meanders on the poleward side of the jet, which are visible in Figure 7b. This cyclonic vortex would have the same rotation direction as jet-induced shear expected on the poleward side. Similarly, anticyclonic relative vorticity is expected on the equatorward side of the Gulf Stream due to the jet-induced shear, and both the FTLE convergence/separation patterns and the sign of vorticity found in inverted U-shaped meanders on this side of the jet in Figure 7b are consistent with that expectation. This alternating FTLE ridge pattern occurs throughout the observation period, propagating eastward with the meanders.

The entrainment and detrainment of flow along the crests and troughs of Gulf Stream meanders is not a new revelation, and is consistent with the model of Bower and Rossby (1989) and Bower (1991), although their model was based on relatively sparse Lagrangian observations. To draw comparison within the diagnostic framework of FTLE, similar analysis was done on a representation of the Bower (1991) kinematic model in the reference frame moving with the same velocity as the phase of the meanders, and is shown in the inset of Figure 7b. In this reference frame, the flow is steady, which has no effect on the FTLE calculation as the method is frame-invariant. For brevity, we refer the reader to the original paper for details of the model and its parameters, which we choose here to be $\lambda = 40$ km, $c_x = 20$ km/d, $A = 50$ km, $L = 400$ km, and $s_c = 100$ km/d, the same as in Figure 7a in Bower (1991). FTLE fields are obtained with an integration time step of 0.5 days and integration time $T = 7$ days. Again, relative vorticity is shown by yellow and green contours, nFTLE ridges are shown in red, and pFTLE ridges are shown in blue. Representative trajectories both forward (cyan) and backward (yellow) in time are included for comparison with the top inset of Figure 7a.

This new approach to analyzing the Bower (1991) model demonstrates that it qualitatively explains many of the LCS jet-bounding patterns found in the SSALTO/DUACS observations. It is clear that the kinematic model is able to explain the alternating FTLE ridges that flank the meandering jet and outline regions of entrainment and detrainment, analogous to those observed just east of Cape Hatteras, 75–68°W. Of course, the Bower (1991) kinematic model does not include any dynamical instability, jet-vortex or vortex-vortex interaction, or pinching off of streamlines associated with formation of Gulf Stream rings. Despite these caveats, the underlying LCS jet-flanking pattern of both the Bower model and the observed, eastward-propagating meander segment of the Gulf Stream are qualitatively similar.

The convergence and divergence of trajectories does not in itself demonstrate mixing in the flanks of the jet, but strongly suggests that it occurs. Rogerson et al. (1999) extended the Bower (1991) model, performing detailed diagnostics on a dynamically consistent numerically modeled flow with very similar characteristics to the Bower (1991) kinematic model. They pointed out that mixing does not occur if the flow is steady in some reference frame, but that an unsteady flow leads to chaotic fluid motions close to the saddle points, leading to an exchange of fluid between the jet and nearby recirculating regions, and between those recirculations and the region beyond. The saddle points in question are sited at the intersection of nFTLE and pFTLE crests in our representation. Thus, we can expect the flanks of the jet to be exchanging fluid with the surroundings in these regions.

This process, being limited to the flanks of the jet, does not permit fluid exchange across the jet axis. It is reminiscent of the unstable jet region in the Waterman and Hoskins (2013) model, where barotropic instability leads to potential vorticity fluxes which erode the flanks of the jet and drive recirculations to either side of it, but do not erode the enhanced potential vorticity gradient at the surface jet axis.

5.2. Dynamics of Coherent Spiral Formation

Aside from the alternating red and blue ridge boundaries of the main jet, another dominant feature of the Gulf Stream LCS is the spiral LCS that are apparent in Figure 7, but not present in the Bower (1991) model. There are many spiral LCS in the vicinity of the Gulf Stream across the span of SSALTO/DUACS data that may equally be examined. As before, there is also a supplementary movie of the equivalent 22 year time series (supporting information Movie S1).

The spiral LCS cover a range of length scales, spanning the mesoscale to submesoscale range. Spiral LCS are not observed at larger length scales, suggesting that the dominant generation mechanism may be a form of shear-flow instability with a long-wavelength cutoff, such as classical barotropic shear-flow instability. Some clear spiral structures may also be seen where there is significant spatial gradient of SST and Chl in the MODIS data (Figure 2). Anticyclonic spirals appear at (72.5°W, 38.5°N), (70°W, 39°N), (68.5°W, 35.5°N), (64.5°W, 39.5°N) and cyclonic spirals appear at (65.5°W, 35.5°N) and (72°W, 37.5°N).

As well as apparently isolated spirals, there are also figure-of-eight spirals seen, for example, near (72°W, 36°N) and (42°W, 48°N) in Figure 8. In 2-D flow, the topological complexification linked to mixing typically produces such patterns, including figures-of-eight (Moffatt, 2001), as in the Duffing oscillator, which Du Toit (2010) also highlighted in the Gulf Stream FTLE structures.

In a seminal paper, Munk et al. (2000) (hereafter, M00) presented observations of mesoscale to submesoscale spiral features first seen in photographs of sunglint on the ocean surface taken on Apollo-Saturn 7 in October 1968. As the nFTLE are attracting ridges in a given flow field, we would expect material collection along them. Therefore, we would expect the M00 spirals to coincide with nFTLE ridges. It is noteworthy that in M00, the observed spirals are "overwhelmingly cyclonic," but in our diagnosis of SSALTO/DUACS observations we observe both cyclonic and anticyclonic spiral nFTLE ridges.

It may not be surprising to observe the prevalence of coherent vortex structures forming and interacting with the Gulf Stream jet. The simplest mechanism for formation, as invoked by M00, is that of the classic Stuart (1967) "Cat's Eye" solution for Kelvin-Helmholtz shear-flow instability. Each flank of the eastward Gulf Stream jet has background relative vorticity that is dominated by the southward gradient of the eastward velocity component, being cyclonic on the poleward flank and anticyclonic on the equatorward flank. The Stuart (1967) mechanism generates vortices with the same sign vorticity as the local background flow shear, thus leading to the presence of cyclonic vortices on the poleward flank and anticyclonic vortices on the equatorward flank. However, the vortices seen in Figure 8 and the full-length movie (supporting information Movie S1) demonstrate that the opposite is also observed. There is an additional process associated with pinching off of Gulf Stream meanders, or vortex shedding from the strongly meandering jet, that is crucial for the transfer of relative vorticity and other features such as warm-core and cold-core rings across the jet.

To illustrate the generation of spiral-like flow features, M00 combine a simple Lagrangian particle tracking method with the Stuart (1967) solution, but these solutions are symmetric—the spirals have the same vorticity as the background on each flank of the jet (may be seen by flipping the sign of the background vorticity in the example in M00)—and one would therefore expect equal numbers of cyclonic and anticyclonic spirals for an axially symmetric jet containing both cyclonic and anticyclonic background shear. To attempt to explain their observed asymmetry, M00 modify the Stuart (1967) solution to include the Coriolis effect and they examine a range of situations with various Rossby numbers. M00 note that cases with and without the Coriolis effect share the same stream function, but in general the Coriolis force modifies the pressure field, which therefore permits modification of flow stability for cyclones/anticyclones.

At zero Rossby number, there is perfect geostrophic balance and flow would follow isobars on an f-plane. For small but nonzero Rossby number, typical of the large-scale flow close to geostrophic balance, the ageostrophic pressure gradient force acts to reinforce the anomalous low pressure associated with cyclonic vortices and acts to dissipate the anomalous high pressure associated with anticyclones. Although M00 emphasize this point in order to explain the prevalence of cyclonic spirals in their observations, their theory also supports stable vortices and spirals of both types when the Rossby number is $\sim$1 or larger. This is the case for strong currents such as the Gulf Stream, where submesoscale dynamics (themselves defined by Ro $\sim$ 1), including processes such as frontogenesis, are known to be important (McWilliams, 1985; Thomas

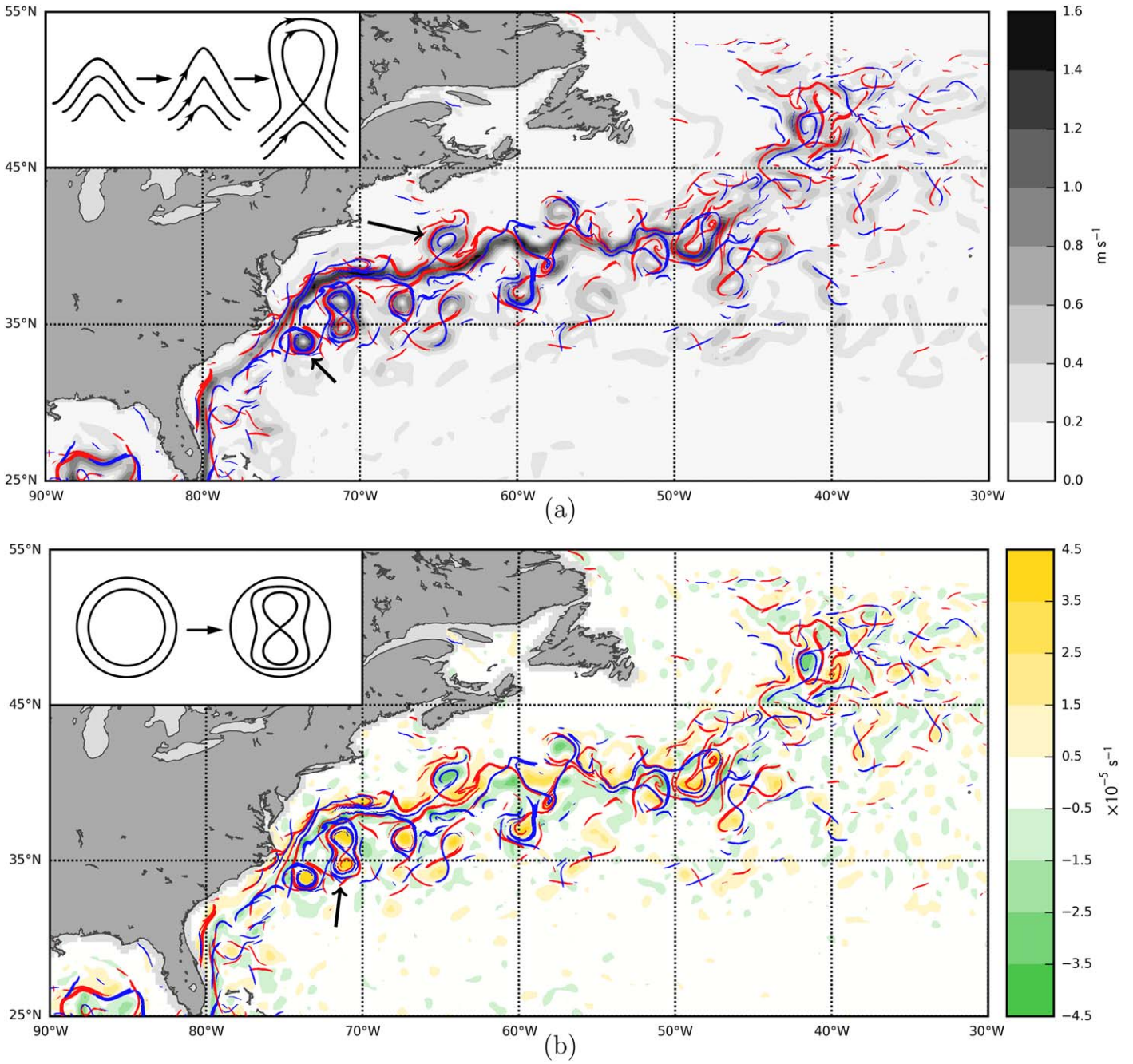

Figure 8. (a) Velocity magnitude and (b) relative vorticity in the Gulf Stream region on 13 November 2000, superimposed with pFTLE (blue) and nFTLE (red) ridges. Top left inset in Figure 8a shows proposed topological change from cusp to recirculating region, adapted from Moffatt (2001). Inset in Figure 8b is a schematic of proposed figure-of-eight flow complexification adapted from Moffatt (2001). Black arrows highlight examples of these topological features in FTLE ridges, whose evolution is supported by supporting information Movie S1, and which contains many more examples in its 22 year sequence.

et al., 2008). Ship sections across the Gulf Stream provide sufficient lateral velocity resolution to capture evidence of Ro $\sim$ 1— see Figure 4 of Joyce et al. (2009). We also note that none of the sunglint spirals observed by M00 appear to be in strong current regions, so one might expect further sunglint observations in these regions to support our diagnosis and for spirals of both types to be present. There do not appear to be compelling examples of anticyclonic sunglint spirals in the NASA Gateway to Astronaut Photography of Earth (http://eol.jsc.nasa.gov) near the Gulf Stream, although the subset of images in this region is rather limited.

5.3. Topological Flow Changes and the Vortex Pinch-off Process

Tracer particles illustrate the connection between the pinch-off process and fluid transfer, but also important are changes to the flow topology during separation and merger of vortex-jet and vortex-vortex. The direct cascade of enstrophy to small scales in turbulence is an important characteristic of geophysical flow. Spectral characteristics of macroscopic ocean turbulence are close to those of idealized 2-D turbulent flow (Salmon, 1998; Held & Larichev, 1996; Danilov & Gurarie, 2000), with a direct enstrophy cascade from the scales of forcing (near the deformation radius, where baroclinic instability is present) toward the small scales of dissipation. Enstrophy is the integral of half of the square of the vorticity (the curl of velocity), so the direct cascade of enstrophy means that the vorticity contour topology becomes more complex at smaller scales. For ideal 2-D turbulence, this direct enstrophy cascade is related to wave triad interactions and the generation of mean-square velocity shear (Kraichnan, 1967), which is consistent with the breakup of eddies due to stirring and eventual viscous dissipation. Insets of Figure 8 show the key topological changes associated with the creation/destruction of pairs of hyperbolic and elliptic fixed points in a 2-D flow (Moffatt, 2001), and events involving similar structures are observed across the 22 year range represented in the supporting information Movie S1, with specific examples in the days before and after the date represented in Figure 8: 13 November 2000. The time direction may be flipped to swap the interpretation between separation and merger. It must be noted that in the aperiodic time-varying system we are studying, these hyperbolic points are not "fixed points" in the same sense, but are hyperbolic trajectories around which the saddle-like behavior evolves. Additionally, FTLE is only capable of identifying the hyperbolic trajectories, but not the elliptic ones. It is for this reason that the elliptic points are also not included in the insets of Figure 8, as their analogs are not available for comparison in the FTLE anyway. One mechanism involving merger of hyperbolic trajectories with the jet is associated with the regular propagation of such features in the ocean interior, from the east of the domain, westward toward the Gulf Stream. These features propagate at a few centimeters per second at a latitude of 35°N, and slower at higher latitude, but are also harder to see outside the Gulf Stream. This appears to match the observed long, baroclinic Rossby wave phase speed (Chelton & Schlax, 1996).

Moffatt (2001) covers a special case of an Euler flow, for which the number of hyperbolic fixed points must equal the number of elliptic fixed points. Topologically, each hyperbolic fixed point in the 2-D Euler flow corresponds to a unique (homoclinic) separatrix that connects back to that fixed point only. Elliptic fixed points are associated with vortices and each new vortex is bound by such a separatrix. Qualitatively at least, the topological flow structures from the Moffatt (2001) model appear to be relevant to the surface geostrophic flow captured by the SSALTO/DUACS observations. Also of relevance is an elegant reduced-gravity modeling study by Poje and Haller (1999), which includes the topology of jet-vortex interaction. It is common to see anticyclonic spirals poleward of the Gulf Stream and cyclonic spirals equatorward (Figures 7 and 8). The supporting information movie of FTLE and vorticity (supporting information Movie S1) confirms that a major process behind this configuration is the growth of large meanders in the Gulf Stream and the pinching off of vortices, transferring vorticity and spiral structures across the jet, although often also involving advection along the jet axis.

Figure 9 shows image sequences around three different days to demonstrate that the vortex pinch-off process is transporting fluid both poleward and equatorward. In all three image sequences, pFTLE (blue) and nFTLE (red) ridges are superimposed on vorticity (green to yellow—scale identical to Figures 7 and 8). Also included are 16 tracer particle locations, represented as black dots in each image. In the days before and after 18 April 2005 (left column), these 16 tracer particles are first identified on the equatorward side of the jet starting on 31 March 2005. By 18 April, the nearby meandering jet has formed an inverted U-shape, and the tracer particles are located in the region within that contains anticyclonic vorticity. After 9, and subsequently 18 days, a hyperbolic trajectory (or saddle; visible where pFTLE and nFTLE ridges cross each other) has appeared beneath the region of fluid that collected under the jet meander, this region has nearly crossed the jet, and all tracer particles remain in its interior. Topological change during this period is also similar to the schematic shown in inset in Figure 8 (top). Over the period 6–22 May 2005 (see supporting information Movie S1) this meander will continue to cross the jet, pinch-off, and transfer its anomalous anticyclonic vorticity into a larger vortex to the north. Most notably, 18 days prior to the meander formation, the tracers show that the fluid was transported from well south of the jet, covering approximately 4° of latitude to become entrained into the jet structure.

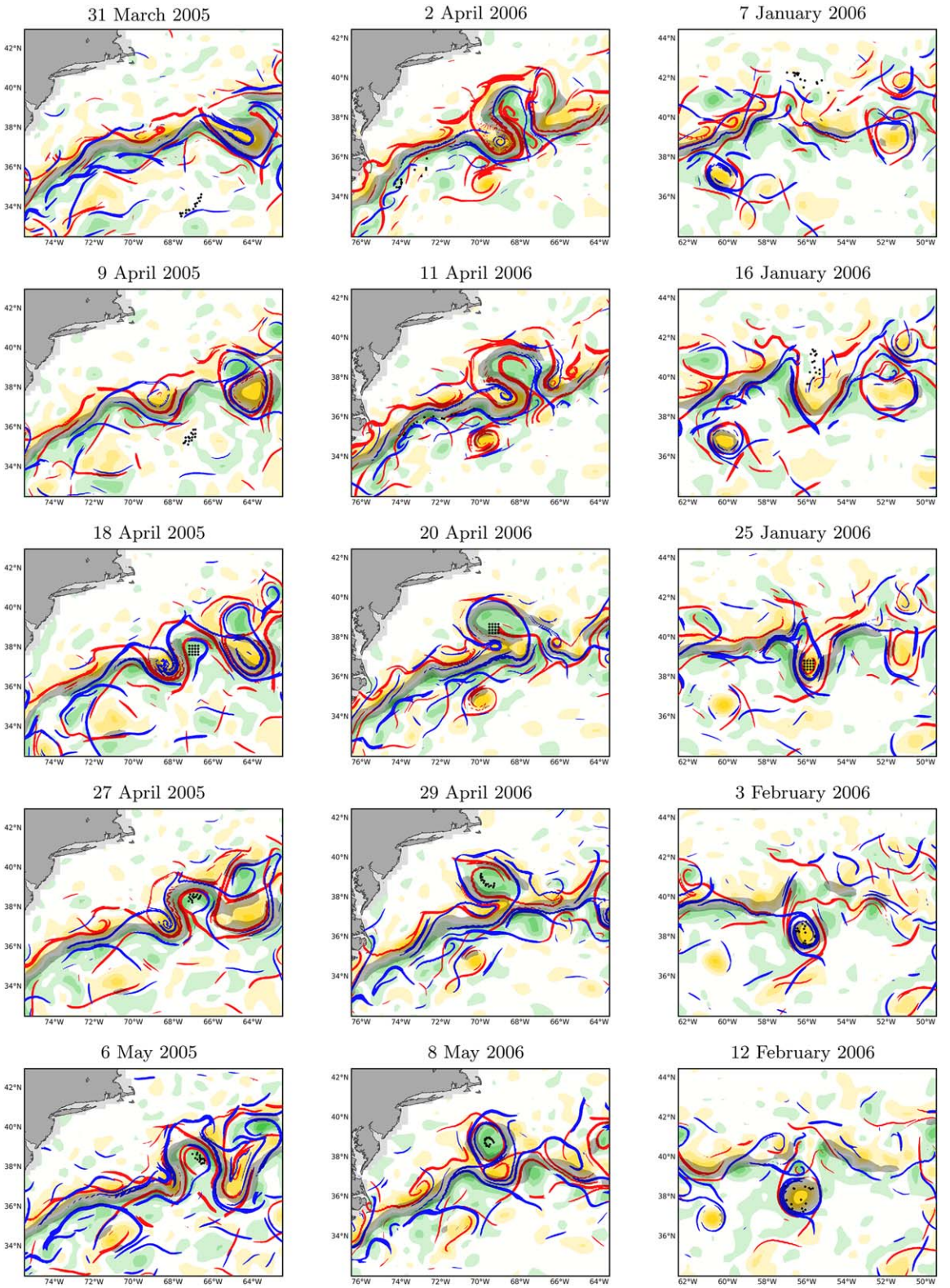

Figure 9. Three sequences of Gulf Stream meander formation/pinch-off and its connection with relative vorticity transfer, ring formation, and FTLE saddle generation. The spatial and temporal regions differ in each column. Relative vorticity is shaded yellow/green with the same scale as in Figure 8. Velocity magnitude is shown in grayscale, for values exceeding 1 m s^{-1}, to reveal the core jet flow where relevant. pFTLE (blue) and nFTLE (red) ridges are overlaid. Each plot contains a set of 16 particles (black dots), initialized from a regular grid in the third row at the central time for each sequence. The three columns show particles entering the jet from the south, crossing the jet from the south, and crossing the jet from the north. A full description is in the text.

Similar fluid transport is observed 2 April to 8 May 2006 (Figure 9, center column). In this case, however, the fluid is not drawn from south of the jet, but shows that a similar pinch-off also occurs with material that has traveled along the jet. On 2 April, the tracer particles can be seen upstream, between 74°W and 72°W, and 34°N and 36°N. That the same transport dynamics are observed with material that traveled along the jet, or was drawn from farther away from the jet, further indicates the efficacy of the Gulf Stream mixing.

To this point, equatorward transport is also observed, and shown in the right column of Figure 9, surrounding 25 January 2006. On that date, 16 tracer particles are shown in the interior of a cyclonic vortex that has been formed as a cusp on the poleward side of the jet. This fluid originated outside of the jet on the poleward side, as can be seen 18 days prior (7 January), and nearly crosses the jet as part of this coherent structure, as can be seen 18 days after (12 February). While material is not observed to exit the Gulf Stream as simply and rapidly as it enters it, this mechanism is observed to repeatedly entrain fluid from well north and south of the jet, and these structures continue to persist and interact with the jet. These three events were selected as examples, but this mechanism was observed repeatedly over the 22 year period, and both poleward and equatorward structure formation and transport is observed across a longitudinal span from approximately 70°W to 50°W.

Our impression from looking at the animated plots is that, whereas the Bower (1991) mechanism explains much of what is seen just downstream of Cape Hatteras (the jet instability region in our classification), fluid exchange across the jet is dominated by pinch-off of large meanders to form rings in both the supercritical wave-maker region just upstream of the NESM, and the subcritical wave-maker region downstream of the NESM. However, on following the trajectories of newly formed rings, it is rare to find one that simply remains on the "wrong" side of the Gulf Stream until it dissipates. Rather, the eddies interact multiple times with the Gulf Stream, often passing back across it rather quickly.

In an attempt to quantify this somewhat, we have used a method similar to that of Andres (2016) to follow the track of the Gulf Stream over time. We do this by identifying a dynamic topography contour to represent the center of the Gulf Stream, and tracking the motion of this contour. Unlike Andres (2016), we prefer to allow the value of dynamic topography chosen to evolve slowly, in order to allow for seasonal and long-term changes in mean dynamic topography over the region. To permit this, we find the dynamic topography values which coincide with a maximum in velocity at each meridional section over the region between 78.5°W and 72.5°W, and average these values on each day. To avoid very rapid fluctuations, we convolve the resulting time series with a Gaussian with full width at half maximum 102 days, which smooths out most variability at time scales shorter than the annual cycle (the annual cycle itself is first fitted and removed, then restored at the end). Then we follow the first contour with this chosen value to be found near the Florida coast, and designate that contour the center of the Gulf Stream.

Figure 10 shows how often the resulting contour passed through each $\frac{1}{12}^{\circ} \times \frac{1}{16}^{\circ}$ (longitude by latitude) grid square, either as a number of instances (days) in the 22 year period for the rare cases, or as percentage of days for the more common cases. It is quite striking how the breadth of the Eulerian mean current seems to represent the envelope of the more frequent paths, suggesting that much of the Eulerian mean width is the result of a broader range of positions of the jet center, rather than a broadening of the actual jet.

When a meander pinches off, the length of the contour suddenly reduces, allowing for the identification of pinch-off events. Similarly, when a ring merges once more with the Gulf Stream, the contour suddenly develops a large meander and therefore its length grows. Based on these events it is possible to identify 372 anticyclonic ring formation events (formation of warm-core rings to the north of the Gulf Stream), and 235 events in which such rings cross back to the south of the Gulf Stream center. These events are shown as red circles (ring creation) and white crosses (ring destruction) in Figure 11, with the symbols marking the position of the saddle point in dynamic topography at the time of creation or destruction. Similarly, blue circles and black crosses mark the sites of creation (248 events) and destruction (231 events) of cold-core, cyclonic rings. The saddle points in this case represent the point in space where the Gulf Stream axis crosses itself at the time of creation or destruction of a ring. This is mathematically equivalent to the point at which a saddle in dynamic topography (defined as having zero first derivative in both x and y directions, and a negative determinant of the Hessian matrix of second derivatives) crosses the Gulf Stream axis contour. Note that saddle points in the dynamic topography are equivalent to those identified using the FTLE diagnostic only in the case of a steady flow.

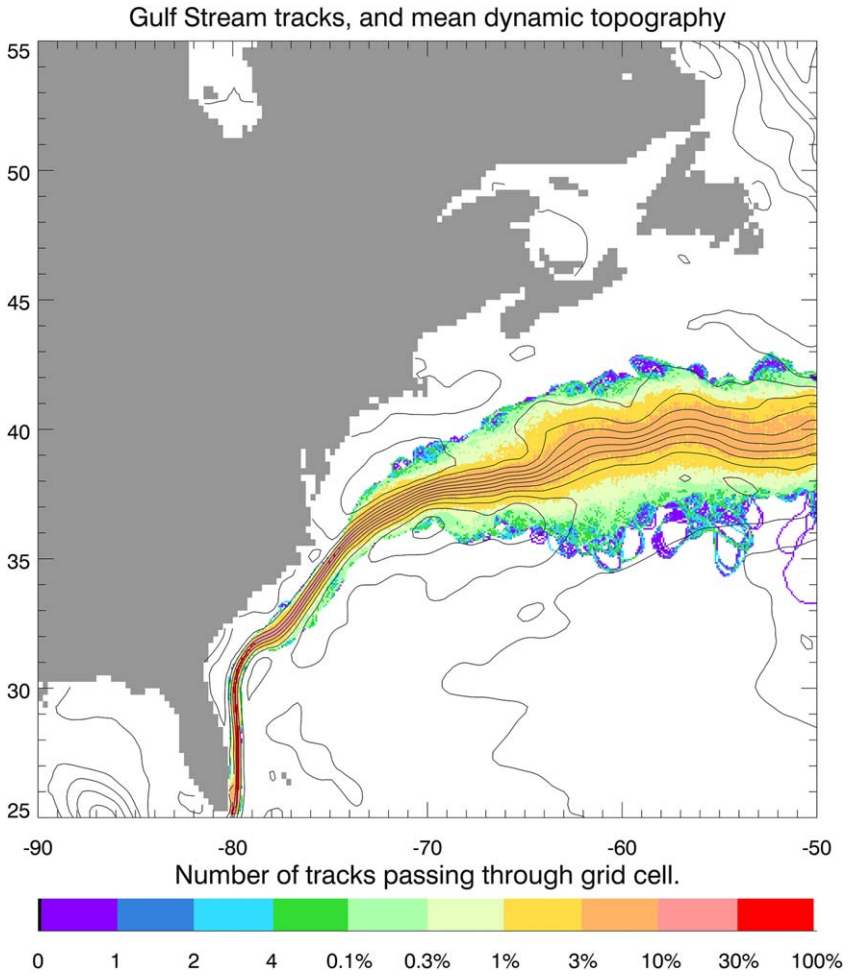

Figure 10. The frequency with which the Gulf Stream center passed through each $\frac{1}{12}^{\circ} \times \frac{1}{16}^{\circ}$ (longitude by latitude) grid square. When expressed as a number, this is the number of days on which this occurred. The larger values represent the percentage of days on which it occurred. Black contours show the mean dynamic topography, with a contour interval of 10 cm.

The visual impression of rapid, multiple interactions is verified by the large fraction of creation events that are complemented by destruction events (especially for cold-core rings), and by the very similar geographical distribution of creation and destruction events.

Ring formation is very rare west of 69°W, but is clear in the region between here and the NESM, which we have identified as the supercritical wave-maker region, as well as in the subcritical wave-maker region downstream of the NESM. Attempts to quantify where the Gulf Stream jet reverses direction compared to its time mean (not shown) give very similar results: the regions of ring formation are the regions where reversals occur.

The two events upstream of Cape Hatteras occur in December 2009, and are the result of a bulge appearing in the center of the Gulf Stream (i.e., a varicose mode rather than the sinuous modes we have focused on here). The Gulf Stream splits into two paths with a slow-moving region between, and then the right hand path strengthens at the expense of the left hand path, expelling the quiescent water to the left of the Gulf Stream. This is a fundamentally different physical mechanism than the vortex pinch-off, and so its representation as red "x" and black "o" markers in Figure 11 should not be interpreted as the creation of warm cores paired with destruction of a cold cores.

The fact that it is rare for a ring to form and then dissipate before drifting back across the Gulf Stream means that the bulk exchange of fluid toward and across the Gulf Stream by a ring should not be

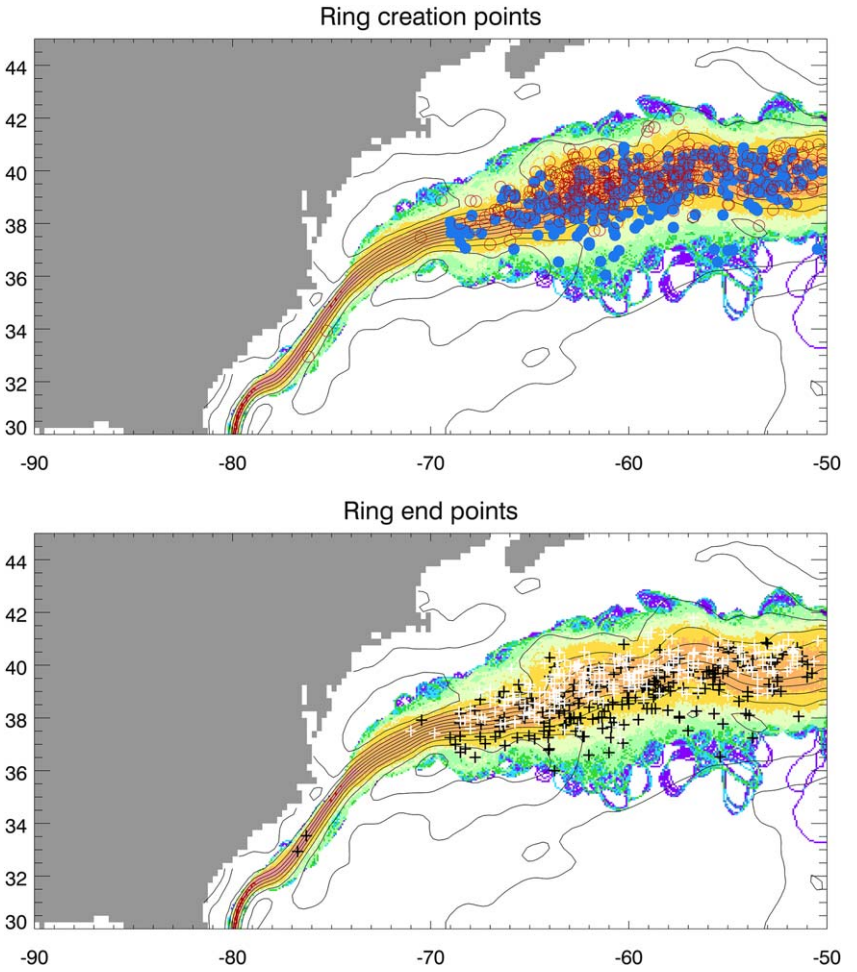

Figure 11. The position of saddle points during the creation and destruction of Gulf Stream rings due to pinch-off of meanders in the Gulf Stream center, or to merger of a ring with the Gulf Stream. Circles mark ring creation (red for warm-core, anticyclonic rings forming north of the Gulf Stream, blue for cold-core, cyclonic rings forming to the south). Crosses mark ring destruction (white for warm-core, black for cold-core). The image beneath is the same as in Figure 10.

considered a strict measure of mixing *across* the Gulf Stream. To measure this particular mixing phenomenon, one could instead consider how much fluid is lost from the ring while it is on the "wrong" side of the Gulf Stream before it is reabsorbed by the jet.

6. Discussion

We have diagnosed FTLE from SSALTO/DUACS absolute geostrophic surface velocity to examine the LCS associated with surface transport and mixing in the Gulf Stream region. This new view highlights the temporal and spatial nonuniformity of Gulf Stream transport and mixing and is related to a range of processes: (i) local entrainment and detrainment from the leading and trailing edges of crests and troughs of eastward-propagating jet meanders, as in the Bower kinematic model, relevant only where and when meanders are propagating eastward; (ii) additional intermittent transport processes involving the dynamics of lateral shear-flow instability and topological flow changes due to pinching off of jet meanders and their associated vortices, which is related to formation of hyperbolic-elliptic trajectory pairs in the flow topology; and (iii) similar topological changes in reverse, related to vortex-jet or vortex-vortex merger.

We have found an interesting relationship between the kinds of Lagrangian process that occur, and the Eulerian picture of vorticity fluxes across the Gulf Stream as discussed in idealized form by Waterman and Hoskins (2013). The Bower model appears to work in the region just downstream of Cape Hatteras,

identified as the jet instability region by Waterman and Hoskins (2013). Here fluid is mixed in the flanks of the jet, but not across the jet. Farther downstream, in what Waterman and Hoskins (2013) call the wavemaker region, strong meanders develop and pinch-off to produce rings, though these rings usually merge again with the jet rather quickly. Both these mechanisms involve the formation of hyperbolic trajectories (saddles) in the flow field, and appear in the current analysis as saddles in both the dynamic topography and the FTLE. The importance of such points, and the chaotic mixing in their vicinity that occurs when the flow is time dependent, was first noted in a similar context by Pierrehumbert (1991).

Poje and Haller (1999) highlighted the topological changes associated with eddy pinch-off and eddy-jet merger in a reduced-gravity shallow water model, including how fluid is often entrained into eddies over a long, thin region known as a "mixing channel." It is interesting that their results carry over to our direct analysis (including FTLE) of the Eulerian velocity field acquired from the surface velocity measurements. We too observe material transport over long distances, caught up in the shear layer of the jet and wound up within eddies (see middle column, Figure 9).

The topological connectivity of hyperbolic trajectories, the material contained in the lobes defined by their connecting separatrices and the movement of these lobes as the flow evolves, has emerged as a new model of transport and mixing known as "lobe dynamics"—see Wiggins (2005), Pratt et al. (2016) for a review. Rogerson et al. (1999) use a barotropic model of a simplified Gulf Stream to explore transport by lobe dynamics. They suggest that transport by lobe dynamics may account for as much Lagrangian fluid exchange along the edge of the jet as the pinch-off process does across the jet (up to ∼5 Sverdrups per meander wavelength, assuming a vertical depth scale of 500 m).

We may use our diagnosed FTLE ridges to examine the size of eddies as they pinch-off, giving a mean diameter of ∼190 km (e.g., second and third columns of Figure 9). Combining this with the number of pinch-off events diagnosed (372 warm-core and 248 cold-core eddies) over the 21.8 year period, together with the same 500 m depth scale gives a mean transport of 7.7 and 5.1 Sv for warm-core and cold-core eddies, respectively. This compares with 1–5 Sv estimated by Rogerson et al. (1999) for transport due to the pinch-off process, although again their estimate is scaled as "per meander wavelength." Comparing our rate of pinch-off (∼17 per year and ∼11 per year for warm-core and cold-core eddies) to that of Rogerson et al. (1999) (5 or 6 per year, per meander wavelength) suggests that the region over which most of the pinch-off occurs spans about 2 or 3 meander wavelengths. This is consistent with the extent of the ring creation points in Figure 11.

Combining our results and those of Rogerson et al. (1999) suggests that transport due to pinch-off could account for ∼5–7 or 2–15 Sv, respectively, and that transport due to lobe dynamics between the recirculation regions (either eddies associated with meanders or eddies which have pinched-off) and the "retrograde region" (the far field, away from the jet) may account for up to 10 or 15 Sv, either poleward or equatorward. Note that this refers to the gross transport rather than the net transport in a particular direction. Knowledge of the gross transport due to these processes would provide a useful measure of whether ocean models are in the correct dynamical regime, with sufficiently vigorous Gulf Stream pinch-off and merger, regardless of the degree to which the meridional volume transport effects cancel in the net.

However, we have also established in this study that there are a similar number of ring creation and destruction events, within the vicinity of the main Gulf Stream. The traditional view of coherent pinched-off eddies carrying fluid large distances across the Gulf Stream and then mixing it remotely appears not to hold. Instead, those eddies recirculate and are reabsorbed into the jet. Although the satellite altimetry data is too coarse to resolve the small scales needed to explicitly diagnose transport with lobe dynamics, it does appear that this process could play a role in transporting material from the pinched-off eddies during the time before they are reabsorbed into the Gulf Stream. It is less clear, however, whether the reabsorbed eddies consistently contain significantly more or less volume—a separate study is required to establish this. A major uncertainty in such a calculation is over the depth scale assumed for the eddies, which may matter more as changes become marginal.

Given that the time-mean Atlantic MOC at 26°N is observed to be ∼17 Sv (McCarthy et al., 2015), and is estimated to be ∼13 Sv at 40°N (Wunsch & Heimbach, 2013), this leads us to an open question of whether or not Gulf Stream pinch-off and lobe dynamics may have an influence on climate. The limited evidence suggests that it may be equally as likely or not that poleward and equatorward components of the volume

transport cancel in the net. The answer will depend on just how much volume is lost from pinched-off eddies before they are reabsorbed into the jet and the degree of asymmetry (in terms of volume changes, not necessarily simply counting number of eddies involved). Due to the upper limit of ~10 Sv magnitude of each component, the implications of this question range from potentially negligible to potentially significant. Only further study will unambiguously resolve the issue. Even if subsequent observational analyses show that the answer is close to zero net transport, ensuring that ocean models correctly simulate the processes behind such net cancelation is also important in order to avoid model bias. A caveat is that little is known observationally about whether circulation east of the Gulf Stream is able to compensate meridional transport processes in the vicinity of the Gulf Stream. At 26°N, it appears that there is little contribution to the Atlantic MOC east of the Gulf Stream (Bryden et al., 2005).

We therefore argue that both pinch-off and lobe dynamics deserve greater scrutiny in climate models, especially as the majority of models do not currently resolve the ocean mesoscale, and remain even further from resolving the submesoscale, where lobe dynamics are more important.

A schematic summarizing the dynamics at play in regions of the North Atlantic in and around the Gulf Stream is shown in Figure 12. Here the transition between the unstable jet and the wave-maker region is displayed in comparison with the transition between supercritical and subcritical flow regimes, and the different jet and eddy dynamics that have been described in the previous literature, and diagnosed directly in this current work. We hypothesize that it is the combination of lobe dynamics with the pinch-off process and the time that detached rings spend on the "wrong side" that characterize the key irreversible transport and mixing process of the Gulf Stream. Lobe dynamics, not explicitly resolved by our FTLE diagnostics, account for material transport globally in an unsteady flow, but efficient mixing (measured in terms of the local rate of change of material property from diffusive stretching and folding due to geophysical turbulence) requires the presence of contrasting local material properties of fluid trapped in lobes. For eddies associated with the troughs and crests of nonbreaking jet meanders, the material properties are usually similar to their local background (e.g., for anomalous vorticity in the Kelvin-Helmholtz instability described by Stuart, 1967 and in the supercritical unstable jet region of the Gulf Stream). Here lobe dynamics (illustrated

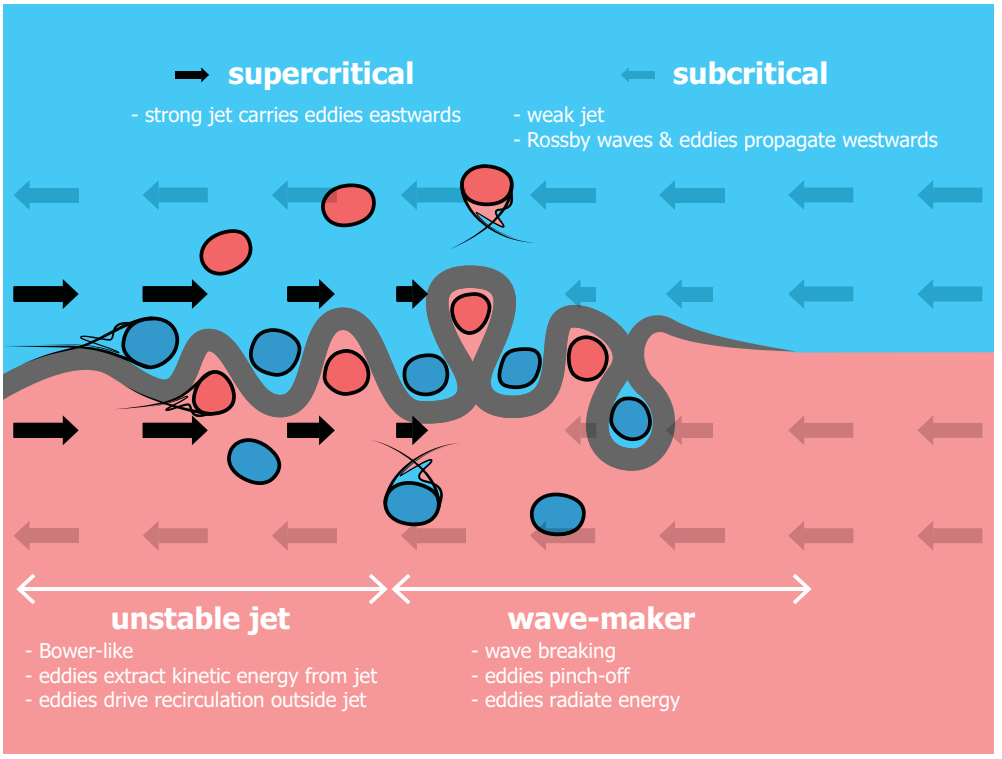

Figure 12. Schematic depicting the relative locations of the described regimes (supercritical/subcritical, unstable jet/wave-maker) and coherent structure dynamics that lead to material transport and mixing in the Gulf Stream.

with solid black lines around the Gulf Stream meanders) transport similar material (blue-blue) or (red-red) toward hyperbolic trajectories and mixing is weak. In contrast, for pinched-off rings or eddies on the "wrong side" of the jet, which begin to appear as the jet transitions from the unstable jet to the wave-maker, the lobe dynamics transport contrasting material (red-blue) or (blue-red), and mixing is strong. It is notable that the time spent by eddies on the "wrong side" may depend significantly on advection within the recirculations which are themselves eddy-driven (see Waterman & Hoskins, 2013 and Figure 5).

There is a suggestion that this phenomenon is a characteristic of many other strong eastward jets that are supercritical with respect to westward-propagating Rossby waves. For example, movies from satellite observations and eddy-resolving ocean general circulation models point to the existence of hot spots where eddies are pinched-off from and reabsorbed into the Antarctic Circumpolar Current (ACC). ACC standing meanders attached to features in seafloor topography (where the jet flow becomes critical, meanders grow and eddies pinch-off) are known to be a source of enhanced eddy kinetic energy and vorticity transfer, and are important for the equilibration of the ACC (Thompson & Naveira Garabato, 2014) and the merging of ACC jets and potential vorticity fronts (Thompson et al., 2010).

The vortices are very often seen to contain spiral LCS at length scales from mesoscale to submesoscale. A plausible generation mechanism is the shear-flow instability theory of M00, involving the wind-up of shear layers. However, unlike the broad view of solely cyclonic spirals put forward by M00, we have argued that both cyclonic and anticyclonic nLCS spirals are seen in the vicinity of the Gulf Stream. Although the theory of M00 supports both types of nLCS spirals where the Rossby number is $\sim$1 or larger, as is true for the smaller and faster flow scales in the Gulf Stream, their observations of sunglint did not capture such examples. The availability of new satellite observations of ocean SST and Chl supports our perspective and provides an independent validation of our diagnosed LCS.

The combination of LCS from satellite altimetry with SST and ocean color observations potentially provides a powerful tool to estimate the state of ocean surface flow and topology, including both regions of high mixing efficiency and the presence of transport barriers, down to the very fine scales of the submesoscale. Similar diagnosis of LCS and ocean tracer fields from climate models may then highlight which model processes need refining to get key features and flow statistics closer to reality. For example, there are typically up to $\sim$30 pinch-off events per year, and although many of these are the same feature pinching off multiple times, the individual events may be counted. It is perhaps not likely that an eddy-resolving ocean model will get individual events to mirror reality, but one might develop a model to simulate the correct number of events per year. LCS identify the boundaries of vortices and jets, so Lagrangian tracking algorithms, like that used in Chelton et al. (2007) may be used to analyze eddy size and propagation, as well as changes to jet position in observations and models.

In terms of aspects already known about the Gulf Stream prior to this study, it was clear that: (i) the Bower kinematic model could explain the observed trajectories of 37 Lagrangian floats over a 21 month study (Bower et al., 1985; Bower, 1991); (ii) eddies were observed to pinch-off from Gulf Stream meanders, predominantly in a particular region (Fuglister & Worthington, 1951); and (iii) that (cyclonic) spiral eddies existed in the ocean (M00). The main results of this study are, in summary: (i) the Bower model of entrainment and detrainment, tested objectively with FTLE against flow from satellite altimetry observations, holds for a 22 year period, but only intermittently and for a limited part of the Gulf Stream; (ii) pinched-off eddies are unlike those associated with the eddies attached to the nonbreaking meanders of the Bower model, as they have anomalous relative vorticity of contrasting sign to the background flow; also, the pinched-off eddies are reabsorbed into the jet after days to weeks and do not systematically escape the jet meridionally; also, the pinch-off region, identified by a combination of Lagrangian and Eulerian methods, corresponds to the wave-maker region of the (Waterman & Hoskins, 2013) model, and the Bower model to the unstable jet region of that model; and (iii) spiral eddies observed objectively by Lagrangian diagnostics are seen to vary intermittently in time (which was not clear from the previous snapshots in M00) and are ubiquitous in our region of study. In contrast to M00, both cyclonic and anticyclonic spiral eddies are shown to exist and we suggest a that this is due to new observations in regions with larger Rossby number. Although our stated focus was on a qualitative rather than quantitative description, we have estimated in this section that the processes of pinch-off and lobe dynamics may each be of comparable gross magnitude to the Atlantic MOC, but we have also posed an open question about whether there may or may not be cancelation in their net meridional transport.

A variety of time scales are present in the diagnosed LCS (see supporting information Movie S1). An in-depth discussion is outside the scope of this study, but we do see spiral rollup (few days to few months; limited by the lifetime of the vortex), meander/vortex growth and pinch-off (few days to a couple of weeks), and hyperbolic (saddle) point propagation in the ocean interior taking about 5 years to cross the basin from east to west. The interplay and intermittency of the complex network of ocean LCS illustrates the structure of ocean transport and mixing, and the wide variety of processes involved. It is reassuring at least that it appears that flow complexity may be created and destroyed by topological changes that are locally simple. Climate simulations of the North Atlantic indicate that the Gulf Stream latitude marks a step-change in the variability and coherence of the Meridional Overturning Circulation (MOC) (Bingham et al., 2007). To link MOC observational programs such as RAPID/MOCHA (http://www.rapid.ac.uk/rapidmoc; www.rsmas.miami.edu/users/mocha) and OSNAP (http://www.o-snap.org) in the subtropical and subpolar gyres, respectively, observation and realistic modeling of Gulf Stream processes is vital. The three-dimensional structure and evolution of the MOC involves connection between the fast, wind-driven circulation of the upper ocean with slower circulation that includes deep western boundary currents and circulation sustained by mixing due to mesoscale eddies and internal waves turbulently cascading to molecular scale, transferring heat and momentum vertically at up to millenial time scales. Diagnosis of evolving LCS in three-dimensional flow is possible and may provide unique insights to the MOC connectivity, extending studies such as Bower et al. (2009). However, the observational constraints for the subsurface velocity are still too weak to diagnose LCS, so we must rely on output from ocean model simulations, perhaps those that assimilate observations. Another significant challenge is the visualization of three-dimensional, evolving LCS for a realistic oceanic flow. Overcoming these challenges could lead us to a better understanding of the transport and mixing hot spots of heat and freshwater throughout the global ocean, which could then guide the development and refinement of ocean observations, just as the previous Lagrangian studies of the ocean with floats and drifters led to extended and refined observational experiments.

Acknowledgments

The altimeter products were produced by SSALTO/DUACS and distributed by AVISO, with support from CNES (http://www.aviso.altimetry.fr/duacs). The FTLE diagnosed in this study from this altimeter data are available from doi:10.5281/zenodo.1145909 (pFTLE) and doi:10.5281/zenodo.1145850 (nFTLE). We thank Norman Kuring for creating the original MODIS SST and Chl images that we adapted. CW is supported by the UK Natural Environment Research Council and the UK-OSNAP project (NE/K010875/1). We also thank the Syracuse University OrangeGrid, supported by National Science Foundation (NSF) award ACI-1341006, for providing computational resources. We are grateful to two anonymous reviewers for their constructive comments, which strengthened this paper. Thanks also to Jöel Hirschi for discussion on the relative contribution to the MOC east of the Gulf Stream.

References

Allshouse, M. R., & Thiffeault, J.-L. (2012). Detecting coherent structures using braids. *Physica D*, *241*(2), 95–105.

Andres, M. (2016). On the recent destabilization of the Gulf Stream path downstream of Cape Hatteras. *Geophysical Research Letters*, *43*, 9836–9842. https://doi.org/10.1002/2016GL069966

Beron-Vera, F. J., Olascoaga, M. J., & Goni, G. J. (2008). Oceanic mesoscale eddies as revealed by Lagrangian coherent structures. *Geophysical Research Letters*, *35*, L12603. https://doi.org/10.1029/2008GL033957

Bingham, R. J., Hughes, C. W., Roussenov, V., & Williams, R. G. (2007). Meridional coherence of the North Atlantic meridional overturning circulation. *Geophysical Research Letters*, *34*, L23606. https://doi.org/10.1029/2007GL031731

Blazevski, D., & Haller, G. (2014). Hyperbolic and elliptic transport barriers in three-dimensional unsteady flows. *Physica D*, *273*, 46–62.

Bower, A. S. (1991). A simple kinematic mechanism for mixing fluid parcels across a meandering jet. *Journal of Physical Oceanography*, *21*(1), 173–180.

Bower, A. S., Lozier, M. S., Gary, S. F., & Böning, C. W. (2009). Interior pathways of the North Atlantic meridional overturning circulation. *Nature*, *459*(7244), 243–247. https://doi.org/10.1038/nature07979

Bower, A. S., & Rossby, T. (1989). Evidence of cross-frontal exchange processes in the Gulf Stream based on isopycnal RAFOS float data. *Journal of Physical Oceanography*, *19*(9), 1177–1190.

Bower, A. S., Rossby, H. T., & Lillibridge, J. L. (1985). The Gulf Stream—Barrier or blender? *Journal of Physical Oceanography*, *15*(1), 24–32.

Bryden, H. L., Longworth, H. R., & Cunningham, S. A. (2005). Slowing of the Atlantic meridional overturning circulation at 25°N. *Nature*, *438*(7068), 655–657. https://doi.org/10.1038/nature04385

Chelton, D. B., de Szoeke, R. A., & Schlax, M. G. (1998). Geographical variability of the first baroclinic Rossby radius of deformation. *Journal of Physical Oceanography*, *28*, 433–460.

Chelton, D. B., & Schlax, M. G. (1996). Global observations of oceanic Rossby waves. *Science*, *272*(5259), 234–238.

Chelton, D. B., Schlax, M. G., Samelson, R. M., & de Szoeke, R. A. (2007). Global observations of large oceanic eddies. *Geophysical Research Letters*, *34*, L15606. https://doi.org/10.1029/2007GL030812

Cornillon, P. (1986). The effect of the New England Seamounts on Gulf Stream meandering as observed from satellite IR imagery. *Journal of Physical Oceanography*, *16*(2), 386–389.

Coulliette, C., Lekien, F., Paduan, J. D., Haller, G., & Marsden, J. E. (2007). Optimal pollution mitigation in Monterey Bay based on coastal radar data and nonlinear dynamics. *Environmental Science & Technology*, *41*(18), 6562–6572.

Danilov, S. D., & Gurarie, D. (2000). Quasi-two-dimensional turbulence. *Physics-Uspekhi*, *43*(9), 863–900.

d'Ovidio, F., Fernández, V., Hernández-García, E., & López, C. (2004). Mixing structures in the Mediterranean Sea from finite-size Lyapunov exponents. *Geophysical Research Letters*, *31*, L17203. https://doi.org/10.1029/2004GL020328

d'Ovidio, F., Isern-Fontanet, J., López, C., Hernández-García, E., & García-Ladona, E. (2009). Comparison between Eulerian diagnostics and finite-size Lyapunov exponents computed from altimetry in the Algerian basin. *Deep Sea Research, Part I*, *56*(1), 15–31.

Du Toit, P. C. (2010). *Transport and separatrices in time-dependent flows* (PhD thesis). Pasadena, CA: California Institute of Technology. Retrieved from http://resolver.caltech.edu/CaltechTHESIS:10072009-165901284

Farazmand, M., & Haller, G. (2012). Computing Lagrangian coherent structures from their variational theory. *Chaos*, *22*(1), 013128.

Fuglister, F. C., & Worthington, L. V. (1951). Some results of a multiple ship survey of the Gulf Stream. *Tellus*, *3*(1), 1–14.

Haller, G. (2002). Lagrangian coherent structures from approximate velocity data. *Physics of Fluids*, *14*(6), 1851–1861.

Haller, G. (2011). A variational theory of hyperbolic Lagrangian coherent structures. *Physica D*, *240*(7), 574–598.

Haller, G., & Beron-Vera, F. (2013). Coherent Lagrangian vortices: The black holes of turbulence. *Journal of Fluid Mechanics*, *731*, R4. https://doi.org/10.1017/jfm.2013.391

Haller, G., & Beron-Vera, F. J. (2012). Geodesic theory of transport barriers in two-dimensional flows. *Physica D*, *241*(20), 1680–1702.

Haller, G., Hadjighasem, A., Farazmand, M., & Huhn, F. (2016). Defining coherent vortices objectively from the vorticity. *Journal of Fluid Mechanics*, *795*, 136–173.

Harrison, C. S., & Glatzmaier, G. A. (2012). Lagrangian coherent structures in the California Current System—Sensitivities and limitations. *Geophysical & Astrophysical Fluid Dynamics*, *106*(1), 22–44.

Held, I. M., & Larichev, V. D. (1996). A scaling theory for horizontally homogeneous, baroclinically unstable flow on a beta plane. *Journal of Atmospheric Sciences*, *53*(7), 946–952. https://doi.org/10.1175/1520-0469(1996)053<0946:ASTFHH>2.0.CO;2

Isern-Fontanet, J., García-Ladona, E., & Font, J. (2006). Vortices of the Mediterranean Sea: An altimetric perspective. *Journal of Physical Oceanography*, *36*(1), 87–103.

Joyce, T. M., Thomas, L. N., & Bahr, F. (2009). Wintertime observations of Subtropical Mode Water formation within the Gulf Stream. *Geophysical Research Letters*, *36*, L02607. https://doi.org/10.1029/2008GL035918

Kraichnan, R. H. (1967). Inertial ranges in two dimensional turbulence. *Physics of Fluids*, *10*(7), 1417–1423. https://doi.org/10.1063/1.1762301

Lekien, F., Coulliette, C., Mariano, A. J., Ryan, E. H., Shay, L. K., Haller, G., et al. (2005). Pollution release tied to invariant manifolds: A case study for the coast of Florida. *Physica D*, *210*(1), 1–20.

Lipinski, D., & Mohseni, K. (2010). A ridge tracking algorithm and error estimate for efficient computation of Lagrangian coherent structures. *Chaos*, *20*(1), 017504. https://doi.org/10.1063/1.3270049

Lipinski, D. M. (2012). *Efficient ridge tracking algorithms for computing Lagrangian coherent structures in fluid dynamics applications* (PhD thesis). Boulder, CO: University of Colorado. Retrieved from http://libraries.colorado.edu/record=b7463239S3

Marshall, J., Shuckburgh, E., Jones, H., & Hill, C. (2006). Estimates and implications of surface eddy diffusivity in the Southern Ocean derived from tracer transport. *Journal of Physical Oceanography*, *36*(9), 1806–1821.

McCarthy, G. D., Smeed, D. A., Johns, W. E., Frajka-Williams, E., Moat, B. I., Rayner, D., et al. (2015). Measuring the Atlantic meridional overturning circulation at 26°N. *Progress in Oceanography*, *130*, 91–111. https://doi.org/10.1016/j.pocean.2014.10.006

McWilliams, J. C. (1985). Submesoscale, coherent vortices in the ocean. *Reviews of Geophysics*, *23*(2), 165–182. https://doi.org/10.1029/RG023i002p00165

Moffatt, H. K. (2001). The topology of scalar fields in 2D and 3D turbulence. In T. Kambe et al. (Eds.), *IUTAM symposium on geometry and statistics of turbulence* (pp. 13–22). Dordrecht, the Netherlands: Kluwer Academic Publishers.

Munk, W., Armi, L., Fischer, K., & Zachariasen, F. (2000). Spirals on the sea, *Proceedings of the Royal Society of London A*, *456*, 1217–1280.

Olascoaga, M. J., Beron-Vera, F. J., Brand, L. E., & Kocak, H. (2008). Tracing the early development of harmful algal blooms on the West Florida Shelf with the aid of Lagrangian coherent structures. *Journal of Geophysical Research*, *113*, C12014. https://doi.org/10.1029/2007JC004533

Olascoaga, M. J., Rypina, I., Brown, M., Beron-Vera, F., Kocak, H., Brand, L., et al. (2006). Persistent transport barrier on the West Florida Shelf. *Geophysical Research Letters*, *33*, L22603. https://doi.org/10.1029/2006GL027800

Onu, K., Huhn, F., & Haller, G. (2015). LCS tool: A computational platform for Lagrangian coherent structures. *Journal of Computational Science*, *7*, 26–36.

Pierrehumbert, R. (1991). Chaotic mixing of tracer and vorticity by modulated traveling Rossby waves. *Geophysical and Astrophysical Fluid Dynamics*, *58*, 285–320.

Poje, A. C., & Haller, G. (1999). Geometry of cross-stream mixing in a double-gyre ocean model. *Journal of Physical Oceanography*, *29*(8), 1649–1665. https://doi.org/10.1175/1520-0485(1999)029<1649:GOCSMI>2.0.CO;2

Pratt, L., Barkan, R., & Rypina, I. (2016). Scalar flux kinematics. *Fluids Barriers CNS*, *1*(3), 27. https://doi.org/10.3390/fluids1030027

Pujol, M.-I., and SL-TAC Team (2017). *Copernicus marine environment monitoring service quality information document* (Tech. rep. CMEMS-SL-QUID-008–032-051). EU Copernicus. France: Mercator Ocean, Ramonville Saint-Agne. Retrieved from http://cmems-resources.cls.fr/documents/QUID/CMEMS-SL-QUID-008-032-051.pdf

Rogerson, A. M., Miller, P. D., Pratt, L. J., & Jones, C. K. R. T. (1999). Lagrangian motion and fluid exchange in a barotropic meandering jet. *Journal of Physical Oceanography*, *29*(10), 2635–2655. https://doi.org/10.1175/1520-0485(1999)029<2635:LMAFEI>2.0.CO;2

Rypina, I. I., Pratt, L. J., & Lozier, M. S. (2011). Near-surface transport pathways in the North Atlantic Ocean: Looking for throughput from the subtropical to the subpolar gyre. *Journal of Physical Oceanography*, *41*(5), 911–925.

Salmon, R. (1998). *Lectures on geophysical fluid dynamics*. New York, NY: Oxford University Press.

Samelson, R. (1992). Fluid exchange across a meandering jet. *Journal of Physical Oceanography*, *22*(4), 431–444.

Shadden, S. C., Lekien, F., Paduan, J. D., Chavez, F. P., & Marsden, J. E. (2009). The correlation between surface drifters and coherent structures based on high-frequency radar data in Monterey Bay. *Deep Sea Research, Part II*, *56*(3), 161–172.

Smith, K. S., & Marshall, J. (2009). Evidence for enhanced eddy mixing at middepth in the Southern Ocean. *Journal of Physical Oceanography*, *39*, 50–69.

Song, T., Rossby, T., & Carter, E. (1995). Lagrangian studies of fluid exchange between the Gulf Stream and surrounding waters. *Journal of Physical Oceanography*, *25*(1), 46–63.

Stuart, J. T. (1967). On finite amplitude oscillations in laminar mixing layers. *Journal of Fluid Mechanics*, *29*(3), 417–440.

Thomas, L. N., Tandon, A., & Mahadevan, A. (2008). Submesoscale processes and dynamics. In M. W. Hecht & H. Hasumi (Eds.), *Ocean modeling in an eddying regime* (pp. 17–38). Washington, DC: American Geophysical Union. https://doi.org/10.1029/177GM04

Thomas, M. D., & Zhai, X. (2013). Eddy-induced variability of the meridional overturning circulation in a model of the North Atlantic. *Geophysical Research Letters*, *40*, 2742–2747. https://doi.org/10.1002/grl.50532

Thompson, A. F., Haynes, P. H., Wilson, C., & Richards, K. J. (2010). Rapid Southern Ocean front transitions in an eddy-resolving ocean GCM. *Geophysical Research Letters*, *37*, L23602. https://doi.org/10.1029/2010GL045386

Thompson, A. F., & Naveira Garabato, A. C. (2014). Equilibration of the Antarctic circumpolar current by standing meanders. *Journal of Physical Oceanography*, *44*(7), 1811–1828. https://doi.org/10.1175/JPO-D-13-0163.1

Waterman, S., & Hoskins, B. J. (2013). Eddy shape, orientation, propagation, and mean flow feedback in western boundary current jets. *Journal of Physical Oceanography*, *43*(8), 1666–1690.

Waterman, S., & Jayne, S. R. (2011). Eddy-mean flow interactions in the along-stream development of a western boundary current jet: An idealized model study. *Journal of Physical Oceanography*, *41*(4), 682–707.

Waugh, D. W., & Abraham, E. R. (2008). Stirring in the global surface ocean. *Geophysical Research Letters*, *35*, L20605. https://doi.org/10.1029/2008GL035526

Wiggins, S. (2005). The dynamical systems approach to Lagrangian transport in oceanic flows. *Annual Review of Fluid Mechanics*, *37*, 295–328.

Williams, R. G., Wilson, C., & Hughes, C. W. (2007). Ocean and atmosphere storm tracks: The role of eddy vorticity forcing. *Journal of Physical Oceanography*, *37*(9), 2267–2289.

Wunsch, C., & Heimbach, P. (2013). Two decades of the Atlantic meridional overturning circulation: Anatomy, variations, extremes, prediction, and overcoming its limitations. *Journal of Climate*, *26*(18), 7167–7186. https://doi.org/10.1175/JCLI-D-12-00478.1